PCCP

Accepted Manuscript

ROYAL SOCIETY OF CHEMISTRY

www.rsc.org/pccp

Physical Chemistry Chemical Physics
CREATED USING THE RSC LaTeX PCCP ARTICLE TEMPLATE – SEE www.rsc.org/electronicfiles FOR DETAILS
ARTICLE TYPE www. rsc.org/xxxxxx | XXXXXXXX

Classical nucleation theory of homogeneous freezing of water: thermodynamic and kinetic parameters

Luisa Ickes,*[a] André Welti,[a] Corinna Hoose,[b] and Ulrike Lohmann[a]

Received Xth XXXXXXXXXX 20XX, Accepted Xth XXXXXXXXX 20XX
First published on the web Xth XXXXXXXXXX 200X
DOI: 10.1039/b000000x

The probability of homogeneous ice nucleation under a set of ambient conditions can be described by nucleation rates using the theoretical framework of Classical Nucleation Theory (CNT). This framework consists of kinetic and thermodynamic parameters, of which three are not well-defined (namely the interfacial tension between ice and water, the activation energy and the prefactor), so that any CNT-based parameterization of homogeneous ice formation is less well-constrained than desired for modeling applications. Different approaches to estimate the thermodynamic and kinetic parameters of CNT are reviewed in this paper and the sensitivity of the calculated nucleation rate on the choice of parameters is investigated. We show that nucleation rates are very sensitive to this choice. The sensitivity is governed by one parameter- the interfacial tension between ice and water, which determines the energetic barrier of the nucleation process. The calculated nucleation rate can differ by more than 25 orders of magnitude depending on the choice of parameterization for this parameter. The second most important parameter is the activation energy of the nucleation process. It can lead to a variation of 16 orders of magnitude. By estimating the nucleation rate from a collection of droplet freezing experiments from the literature, the dependence of these two parameters on temperature is narrowed down. It can be seen that the temperature behavior of these two parameters assumed in literature does not match with the predicted nucleation rates from the fit in most cases. Moreover a comparison of all possible combinations of theoretical parameterizations of the dominant two free parameters show that one combination fits the fitted nucleation rates best, which is a description of the interfacial tension coming from a molecular model [Reinhardt and Doye, *J. Chem. Phys.*, 2013, *139*, 096102] in combination with an activation energy derived from self-diffusion measurements [Zobrist *et.al., J. Phys. Chem. C*, 2007, *111*, 2149]. However, some fundamental understanding of the processes is still missing. Further research in future might help to tackle this problem. The most important questions, which need to be answered to constrain CNT, are raised in this study.

1 Introduction

Since the first freezing experiments of Fahrenheit in 1753, many studies have elaborated the phase transition of supercooled water. Various experiments revealed that the freezing temperature of pure water droplets has a strong dependence on the droplet size. While droplets 1 cm in diameter freeze at 240 K, 1 μm droplets remain liquid down to 233 K. To a smaller extent exposure time of droplets at a certain temperature influences the probability of droplet freezing. A higher cooling rate also lowers the freezing temperature for a given droplet size. These observations can be well captured by Classical Nucleation Theory (CNT; here CNT always refers to Classical Nucleation Theory of freezing and not nucleation of particles from the gas phase), where the freezing process is described stochastically based on thermodynamic and kinetic parameters[1].

When CNT was initially developed, our knowledge about supercooled water and its characteristics was not sufficient[2]. Even today, there is still no complete physical model for liquid water, which takes into account all its unusual properties[3] to constrain the theory. Therefore, there are thermodynamic and kinetic parameters in CNT where a comprehensive description is not available or at least not known over a broad temperature range. These unconstrained parameters are a major source of the uncertainties in the nucleation rates derived by CNT. As an example, the interfacial tension between water and ice σ_{iw} has not been measured below 273.15 K. This introduces major uncertainties in the energy barrier ΔG.

To reconcile CNT with the outcome of laboratory measurements, several approximations of thermodynamic and kinetic parameters have been proposed on the basis of indirect measurements or theoretical considerations[4]. On the one hand, studies have focused on kinetics by adapting the kinetic prefactor, *e.g.* Hagen *et al.*[5], Pruppacher[2] and Huang and Bartell[6], and on the other hand focused on thermodynamics by changing the interfacial free energy, *e.g.* Eadie[7]. These

[a] *Institute of Atmospheric and Climate Science, ETH Zurich, Universitätstrasse 16, Zurich, Switzerland. Tel: +41 44 632 7369; E-mail: luisa.ickes@env.ethz.ch*
[b] *Institute for Meteorology and Climate Research, Karlsruhe Institute of Technology, Karlsruhe, Germany.*

different approaches have led to multiple formulations of the unconstrained CNT parameters and the theory itself.

The aim of this paper is to clarify and compare different formulations of CNT currently used in the research community. CNT is used in different research fields with many applications, e.g. biology, food industry and atmospheric sciences[8]. The focus will be on atmospheric applications in this study. However, the theory itself and findings might also be important for other fields.

The freezing of small water droplets has a major influence on atmospheric cloud formation and the physical properties of clouds. Three major cloud types can be defined in terms of the phase: i) water clouds, consisting of water droplets only, ii) mixed-phase clouds, consisting of both ice and water particles, and iii) ice clouds, consisting of ice crystals. Ice in clouds may form via homogeneous or heterogeneous ice nucleation mechanisms, depending on the temperature and supersaturation. In the absence of sufficient ice nuclei homogeneous nucleation is the dominant process in cirrus clouds as well as anvils of deep convective clouds at low temperature conditions. Heterogeneous nucleation is the dominant process for mixed-phase clouds and is initiated above the homogeneous freezing temperature (approx. 235 K) by impurities in the water droplets. Comprehensive definitions of heterogeneous nucleation mechanisms can be found in Vali[9]. However, the focus of this study is on homogeneous nucleation.

The net radiative effect of a cloud depends on its physical properties like temperature, vertical and horizontal extent, optical thickness and phase and is therefore sensitive to freezing processes. The analysis presented in this study will help to develop CNT-based parameterizations of freezing in regional and global climate models to improve the representation of cirrus clouds and anvil formation of deep convective clouds.

In the following section 2 the formalism of CNT and the thermodynamic and kinetic concepts making up CNT are introduced before sections 3 and 4 examine the different thermodynamic and kinetic parameters and summarize the physical considerations or assumptions they are based on. The associated uncertainties are discussed in detail in section 5.

In section 6 we compare CNT, using the parameterizations for the thermodynamic and kinetic parameters as proposed by different authors, to measured homogeneous nucleation rates from 33 droplet freezing experiments using a variety of experimental techniques (Table 4). This comparison enables to check the validity of different theoretical estimates of the two most important unconstrained parameters. This gives an indication which formulations are able to quantitatively reproduce laboratory data.

2 Classical Nucleation Theory

The key concepts and equations of CNT are summarized here. For details we refer to Volmer and Weber[1], Turnbull and Fisher[10], Fletcher[11], Dufour and Defay[12], Young[13], Debenedetti[14], Pruppacher and Klett[15] and references therein.

Statistical fluctuation of molecules in supercooled liquid due to thermal vibration can lead to spontaneous formation of ordered solid molecule clusters, called ice embryos. The size of an embryo fluctuates as individual water molecules (monomers) are gained or lost from liquid phase. However, at a certain critical embryo size additional incorporation of further water molecules to the crystal lattice becomes thermodynamically favored. This critical embryo (ice germ) may then allow the entire parent phase (supercooled liquid) to undergo a macroscopic phase transition: the droplet freezes.

CNT aims to describe this freezing process theoretically, in terms of a temperature-dependent nucleation rate [m^{-3} s^{-1}] by a thermodynamic and a kinetic component (*i.e.* the temperature and pressure dependent energy barrier of spontaneous cluster formation and the rate of molecule incooperation into existing clusters). This nucleation rate can be understood as the formation rate of ice germs in a volume of water leading to freezing over time.

2.1 Thermodynamics of nucleation

The thermodynamic part of the nucleation rate gives the number of ice germs formed per unit volume of water at a given temperature. The formation of a spherical ice embryo in the liquid phase requires a decrease in entropy, and may form a barrier to nucleation. The corresponding change in Gibbs energy required to form an ice embryo containing n_k water molecules (ΔG_k) forms an energy barrier to nucleation. This barrier must be overcome when creating a spherical ice embryo in the liquid phase. It consists of a volume term and a surface term and can be derived by integrating the first law of thermodynamics for the thermodynamic potential G giving the following expression:

$$\Delta G_k = \underbrace{n_k \cdot [\mu_\mathrm{i}(T) - \mu_\mathrm{w}(T)]}_{\text{volume term}} + \underbrace{4\pi r_\mathrm{embryo}^2 \sigma_\mathrm{iw}(T)}_{\text{surface term}}, \qquad (1)$$

where n_k is the number of water molecules in the ice embryo, $\mu_{\mathrm{w,i}}(T)$ the chemical potential of the water/ice phase as a function of temperature, r_embryo the radius of an assumed-spherical ice embryo (discussed further below) and σ_iw denotes the interfacial tension between ice and water.

The first term in Eq. (1) (volume term) describes the decrease in chemical potential experienced by the embryo, relative to the parent phase due to the phase transition. This de-

crease can be expressed as a function of temperature and supersaturation with respect to ice (S_i):

$$\mu_i(T) - \mu_w(T) = -k_B T \ln\left(\frac{e_{sw}(T)}{e_{si}(T)}\right) = -k_B T \cdot \ln S_i \ , \quad (2)$$

where k_B is the Boltzmann constant and S_i denotes the ratio of the saturation vapour pressures over water (e_{sw}) and ice (e_{si}). The number of water molecules in the ice embryo can be calculated from the ratio of the volume of the embryo and the volume of a water molecule in ice [$v_{ice}(T)$]:

$$n_k = \frac{4\pi}{3} \cdot \frac{r_{embryo}^3}{v_{ice}(T)} \ . \quad (3)$$

In Eq. (3) $v_{ice}(T)$ can be calculated from the density of ice, which *e.g.* can be found as an empirical temperature dependent function in Pruppacher and Klett[15] [Eq. (3.2)]. Using Eq. (2) and Eq. (3) the volume term can be expressed as:

$$n_k \cdot [\mu_i(T) - \mu_w(T)] = \frac{4\pi}{3} \cdot \frac{r_{embryo}^3}{v_{ice}(T)} \cdot (-k_B T \cdot \ln S_i) \ . \quad (4)$$

The second term in Eq. (1) (surface term) describes the energy needed to form the interface of the embryo. The formulation is based on the assumption that the ice embryo is spherical, with an interfacial tension similar to a macroscopic system (*e.g.* Anisimov[16]). In addition, it is usually assumed that the curvature effect on interfacial tension is neglected by assuming that the curvature radius is considerably larger compared to the molecular dimensions (capillary assumption)[17]. Especially for small clusters, these assumptions may be violated and are major limitations for CNT.

The critical size of an ice embryo (*i.e.* germ size) is a function of temperature and supersaturation (or saturation ratio). It has been calculated using two different approaches. In the first, the critical germ radius is defined as the maximum of the energy barrier ΔG (*i.e.* at the equilibrium between the volume and surface term), resulting in

$$r_{germ} = \frac{2 v_{ice} \sigma_{iw}}{k_B T \ln\left(\frac{e_{sw}}{e_{si}}\right)} = \frac{2 v_{ice} \sigma_{iw}}{k_B T \ln S_i} \ . \quad (5)$$

In the second approach, the equilibrium condition for the ice germ in a supercooled droplet of pure water which itself is in equilibrium with humid air [Pruppacher and Klett[15]; Eq. (6.10) and (6.52)] is integrated. This approach becomes equivalent to the first, if the saturation ratio is expressed as a function of the latent heat of melting L_m [*e.g.* Rogers and Yau[18], Eq. (2.15)]:

$$S_i = \exp\left(\frac{L_m}{k_B T} \cdot \frac{T_0 - T}{T}\right), \quad (6)$$

where $T_0 = 273.15$ K.
Other formulations for r_{germ}, taking solution and curvature effects into account, can for example be found in Khvorostyanov and Sassen[19], Khvorostyanov and Curry[20] and Jeffery and Austin[3].

Eqs. (4) and (5) can be inserted into Eq. (1) to predict the energy barrier ΔG to ice germ formation as:

$$\Delta G = \frac{16\pi}{3} \cdot \frac{v_{ice}^2 \sigma_{iw}^3}{(k_B T \ln S_i)^2} \ . \quad (7)$$

The temperature and saturation dependent number of ice germs (N_{germ}) per unit volume of water can be expressed in form of a Boltzmann distribution using ΔG [Eq. (7)]:

$$N_{germ}[m^{-3}] = N_l \cdot \exp\left(-\frac{\Delta G}{k_B T}\right) , \quad (8)$$

where N_l is the volume-based number density of water molecules in the liquid parent phase.

2.2 Kinetics of nucleation

The kinetic part of the nucleation rate gives the number of water molecules, which can potentially be incorporated into the ice germ. The flux of water molecules available for incorporation into an ice germ must be taken into account in order to estimate a nucleation rate. This flux can be understood as the diffusive flux (Φ), which can be expressed as a Boltzmann distribution:

$$\Phi = \frac{k_B T}{h} \cdot \exp\left(-\frac{\Delta g^{\#}}{k_B T}\right) , \quad (9)$$

where h denotes the Planck's constant and $\Delta g^{\#}$ the activation energy for the transfer of a water molecule across the water-ice boundary [cf. section 3.1, Eq. (14)-(16)]. Φ can be interpreted either as the frequency at which water molecules overcome the activation energy barrier[21], as a rate of collisions or as a probability of bond breaking and molecular reorganisation[15].

A second kinetic prefactor, the Zeldovich factor Z, accounts for the depletion of the cluster population due to germ production[22]. This factor embodies the non-equilibrium of the kinetic process and has a value between 10^{-2} and 1, where a value of 1 means that equilibrium is assumed. The estimation of Z is discussed further in section 3.2.2.

Using the described expressions for the diffusive flux Φ and the kinetic prefactor Z the rate K at which water molecules are transferred into an ice germ can be predicted by

$$K = n_s \cdot 4\pi r_{germ}^2 \cdot Z \cdot \Phi \ , \quad (10)$$

where n_s is the number of molecules in jumping distance around the germ surface/neighboring the germ surface and $4\pi r_{germ}^2$ is the surface area of the critical ice germ (see section 3.2.1).

2.3 Nucleation rate

Combining the thermodynamic [Eq. (8)] and the kinetic part [Eq. (10)], a formulation of the steady state nucleation rate can be expressed as:

$$J_{\mathrm{hom}}[\mathrm{m}^{-3}\cdot\mathrm{s}^{-1}] = \underbrace{K}_{\text{Kinetics}} \underbrace{\cdot N_{\mathrm{l}}\cdot\exp\left(-\frac{\Delta G}{k_{\mathrm{B}}T}\right)}_{\text{Number of germs}} \quad (11)$$

Inserting Eq. (10) and Eq. (9) into Eq. (11) leads to:

$$\begin{aligned} J_{\mathrm{hom}}[\mathrm{m}^{-3}\cdot\mathrm{s}^{-1}] &= n_{\mathrm{s}}\cdot 4\pi r_{\mathrm{germ}}^2\cdot Z\cdot\Phi\cdot N_{\mathrm{l}}\cdot\exp\left(-\frac{\Delta G}{k_{\mathrm{B}}T}\right) \\ &= n_{\mathrm{s}}\cdot 4\pi r_{\mathrm{germ}}^2\cdot Z\cdot\frac{k_B T}{h}\cdot\exp\left(-\frac{\Delta g^{\#}}{k_{\mathrm{B}}T}\right) \\ &\quad \cdot N_{\mathrm{l}}\cdot\exp\left(-\frac{\Delta G}{k_{\mathrm{B}}T}\right) \end{aligned} \quad (12)$$

The variables N_{l}, n_{s}, Z, the surface area of the ice germ and the prefactor $k_{\mathrm{B}}T/h$ of the flux Φ are summarized as the pre-exponential factor C_{prefac} (see section 3.2):

$$J_{\mathrm{hom}}[\mathrm{m}^{-3}\cdot\mathrm{s}^{-1}] = \underbrace{C_{\mathrm{prefac}}}_{\substack{\text{preexp.}\\ \text{factor}}} \cdot\exp \underbrace{\left(-\frac{\Delta g^{\#}}{k_{\mathrm{B}}T}\right)}_{\substack{\text{kinetic}\\ \text{exponent}}} \cdot\exp \underbrace{\left(-\frac{\Delta G}{k_{\mathrm{B}}T}\right)}_{\substack{\text{thermodynamic}\\ \text{exponent}}} . \quad (13)$$

In sections 3 and 4 uncertainties associated with the individual unconstrained components of Eq. (13) are analyzed and evaluated in section 5 and 6.

3 Uncertainties in the kinetics

3.1 Activation energy ($\Delta g^{\#}$)

The activation energy ($\Delta g^{\#}$) describes the energy required for a single molecule to diffuse across the water-ice boundary, in addition to the free energy barrier ΔG. $\Delta g^{\#}$ can be understood as the activated state through which a molecule must pass when diffusing from the parent phase to the embryo of the new phase [10].

It is difficult to perform direct measurements from which to determine $\Delta g^{\#}$. Various estimation methods have been applied and have yielded in diverse findings. Nevertheless, the following independent characteristics of $\Delta g^{\#}$ can be stated:

- The diffusion of a water molecule from the liquid phase into the ice lattice requires the breaking of hydrogen bonds between the diffusing water molecule and its neighbors. After breaking loose (one or two hydrogen bonds may be retained) the molecule is influenced by the force field of the surrounding water molecules and moves across the interface.
  The breaking of hydrogen bonds increases the internal energy of the diffusing water molecule, allowing it to overcome $\Delta g^{\#}$ [23]. Therefore $\Delta g^{\#}$ depends on the number of hydrogen bonds connecting a given water molecule to its neighbors, which is dependent on the structure of the water (hydrogen bond network of the water molecules). Below 310 K, a water molecule is expected to possess an average of three tetrahedrally-arranged hydrogen bonds [23].

- As diffusion depends on temperature, so does the activation energy. $\Delta g^{\#}$ increases with decreasing temperature, because the average number of hydrogen bonds in a network of supercooled water molecules increases with decreasing vibrational energy [15]. Hydrogen-bond strength increases with decreasing temperature and the structure of the water itself becomes more ice-like at lower temperature [24,25]. Bulavin *et al.* [23] showed that self-diffusion in water is based on the movement of single water molecules (one-particle contribution) near 273.15 K. At low temperatures the collective contribution of self-diffusion might become more important. Therefore Hagen *et al.* [5] proposed a contrary temperature dependence below 241 K. They argue that below this temperature the diffusion process is a cooperative phenomenon and ice embryos grow by transfer of increasingly large water clusters instead of monomers. Consequently less hydrogen bonds – only the ones at the cluster periphery – have to be broken.

There are three measurable quantities (defined by the Glasstone relations [3,26]) based on which the activation energy $\Delta g^{\#}$ can be estimated: the viscosity of water η, the self-diffusivity of water D and the dielectric relaxation time τ of water:

$$\eta = \eta_0\cdot\exp\left(\frac{\Delta g_{\eta}^{\#}(T)}{RT}\right) \quad (14)$$

$$D = D_0\cdot\exp\left(-\frac{\Delta g_{\mathrm{D}}^{\#}(T)}{RT}\right) \quad (15)$$

$$\frac{1}{\tau} = \frac{k_{\mathrm{B}}T}{h}\cdot\exp\left(-\frac{\Delta g_{\tau}^{\#}}{k_{\mathrm{B}}T}\right). \quad (16)$$

Measurements of Krynicki *et al.* [27] showed that $\Delta g_{\eta}^{\#}$ and $\Delta g_{D}^{\#}$ are around $19\cdot 10^3$ J mol^{-1} near the melting point. Wang

et al. [28] estimated $\Delta g^{\#}_{\eta}$, $\Delta g^{\#}_{D}$ and $\Delta g^{\#}_{\tau}$ at 298.15 K and proposed that the activation barrier is the same for viscous flow, self-diffusion and dipole orientation with breaking approximately two hydrogen bonds. However, it has not been proven that all three relations are physically correct, nor that $\Delta g^{\#}_{\eta}$, $\Delta g^{\#}_{\mathrm{D}}$, $\Delta g^{\#}_{\tau}$ are equal. The possibility of $\Delta g^{\#}$ depending on the measured quantity is beyond the scope of this work. Thus $\Delta g^{\#}$ is used in the following for the activation energy independent of the measurable quantity the estimation is based on.

The value of $\Delta g^{\#}$ derived from different analyzes varies with the input data as well as the applied fitting method. Eight different descriptions of $\Delta g^{\#}$ from Dufour and Defay [12], Eadie [7], Young [13], Pruppacher and Klett [15], Jeffery and Austin [3], Khvorostyanov and Sassen [19], Khvorostyanov and Curry [20], Zobrist *et al.* [29] and Chen *et al.* [30] are shown in Fig. 1 as a function of temperature. The methods and datasets used are summarized in Table 1 and described in detail in appendix A.

The different $\Delta g^{\#}$ in Fig. 1 spread over almost one order of magnitude. This spread leads to an even larger variation in the predicted nucleation rate J_{hom}, as $\Delta g^{\#}$ is found in the exponential term of Eq. (9). Notably, the expression of Khvorostyanov and Curry [20] has an opposite temperature dependence to the other formulations below 243.15 K, so that the difference in $\Delta g^{\#}$ is the largest in this temperature regime. This difference can be traced to a lack of understanding of the change in water structure bonding at low temperatures.

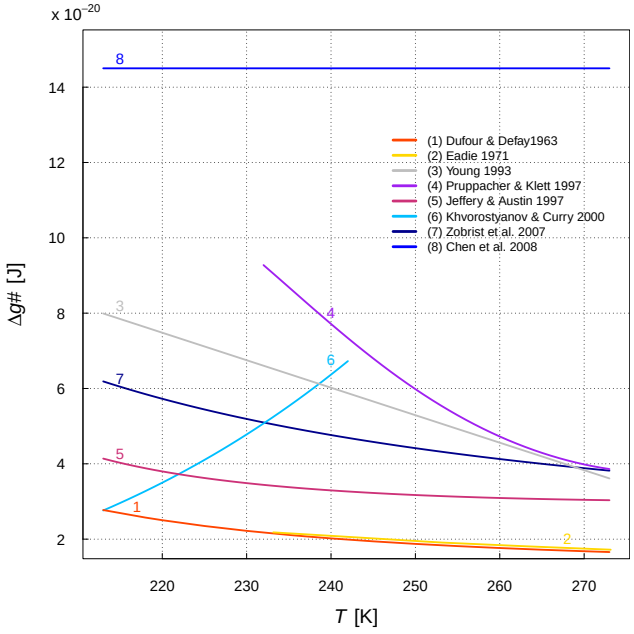

Fig. 1 Variation of the activation energy $\Delta g^{\#}$ with temperature T; Figure modified from Hoose and Möhler [31].

Table 1 Summary of methods for estimating $\Delta g^{\#}$

Theory	$\Delta g^{\#}$ based on	Dataset	Comments
Dufour & Defay 1963	viscosity	Huber et al. 2009; (Dorsey 1940)	
Eadie 1971	dielectric relaxation time	Collie et al. 1948	
Young 1974	viscosity and homogeneous freezing data	Hallett Hagen and Anderson 1981	
Pruppacher& Klett 1997	self-diffusivity	Mils 1971, 1973; Gillen et al. 1972; Pruppacher 1972	T >233.15 K
Jeffery & Austin 1997	self-diffusivity	Prielmeier et al. 1987; Harris and Wolf	
Khvorostyanov & Curry 2004	homogeneous freezing data	similar to Jensen et al. 1994 (Hagen et al. 1981; DeMott and Rogers 1990)	T <243.15 K
Zobrist et al. 2007	self-diffusivity	Smith and Kay 1991	
Chen et al. 2008	fit parameter	-	

3.2 Prefactor (C_{prefac})

In this section the different values of the variables comprising C_{prefac}, which is the prefactor in front of the energy barriers in Eq. (13), are listed. We emphasize that the definition of C_{prefac} is not the same definition as used by all authors. Moreover some authors estimated C_{prefac} as a single quantity to simplify the calculation. The sensitivity of J_{hom} to the parameters discussed in this section is evaluated in section 5.

3.2.1 Number of water molecules in contact with the unit area of an ice germ (n_{s}) and volume number density of water molecules in liquid water (N_{l}). n_{s} has been estimated as a temperature-independent value by different authors between $5.85 \cdot 10^{18}$ m^{-2} and $1 \cdot 10^{19}$ m^{-2}. See Appendix B for details.

The factor N_{l} accounts for the fact that homogeneous nucleation is a volume dependent process. The variation of this parameter in literature estimates is not as large as in the case of n_{s}. In Tabazadeh *et al.*[32], the number density of water molecules in a solution droplet of 1 m^{-3} is given as $3.35 \cdot 10^{28}$ m^{-3} consistent with Jacobi[33], who reported $3.33 \cdot 10^{28}$ m^{-3}, whereas in Zobrist *et al.*[29] a slightly lower value of $3.1 \cdot 10^{28}$ m^{-3} is used.

3.2.2 Zeldovich factor (Z). Z represents the non-equilibrium nature of an ice-nucleating system (*i.e.* ice embryos plus parent phase). It accounts for the loss of subcritical clusters in the embryo population due to the growth of ice embryos, which reduces the number of water molecules available to transfer across the water-ice interface. If an equilibrium is assumed, Z has the value 1. Otherwise, Z can be estimated as follows:

$$Z = \frac{1}{n_{k,\mathrm{germ}}} \cdot \sqrt{\frac{\Delta G}{3\pi k_{\mathrm{B}} T}} \,. \qquad (17)$$

Whereas Fletcher[11] states that the effect of taking Z into account is minor, Pruppacher and Klett[15] reckon that Z has the order of 10^{-1} and Butorin and Skripov[34] estimate Z to be of the order of 10^{-2}.

3.2.3 Estimates of the total prefactor C_{prefac}. By coincidence, the product of n_{s}, the germ surface area A, and Z is approximately equal to unity. Therefore the total prefactor is approximately the product of the volume number density N_{l} and the temperature dependent term $k_{\mathrm{B}}T/h$. Fletcher[11], Young[13] and Debenedetti[14] for example approximate the prefactor for homogeneous freezing by 10^{41} m^{-3}s^{-1} over the whole temperature range.

4 Uncertainties in the thermodynamics

4.1 Interfacial tension between ice and water (σ_{iw})

The interfacial tension between ice and water (σ_{iw}) is an important but poorly-constrained parameter in CNT [cf. Eq. (7)]. σ_{iw} is strongly temperature-dependent, due to the temperature dependence of the structure of water. With decreasing temperature, the structure of water becomes increasingly ice-like[24,25], decreasing the ice-water interfacial entropy (ordering of water molecules in contact with the ice structure increases) and thus σ_{iw}. The interfacial free energy, and thus the interfacial entropy, becomes zero in the limiting case where the water structure is completely isomorphic with ice[35].

Direct measurements of σ_{iw} for ice embryos is nearly impossible, as they may be smaller than 1 nm[29]. Moreover, metastable supercooled water tends to freeze heterogeneously on any experimental apparatus. Therefore σ_{iw} is normally measured at or above 273.15 K using macroscopic water drops. These measurements are then extrapolated to ice embryos in supercooled water. This approach implicitly assumes that the ice embryos have the same intensive properties as bulk water. In addition, the extrapolation of σ_{iw} to supercooled temperatures requires theoretical assumptions about its temperature dependence. These assumptions introduce significant uncertainty to the result. Alternatively the interfacial tension between ice and water can be estimated by using molecular models or based on fitting of CNT to measured nucleation rates.

Several different estimates of σ_{iw} are summarized in Fig. 2 as a function of temperature. The figure includes measurements of σ_{iw} at 273.15 K ($\sigma_{\mathrm{iw},0}$) and their theoretical extrapolations as just described, theoretical estimates of $\sigma_{\mathrm{iw},0}$ and $\sigma_{\mathrm{iw}}(T)$, as well as results from molecular models and results from fits of CNT. Table 2 gives the methods and datasets used in each of these studies. See Appendix C and D for more details.

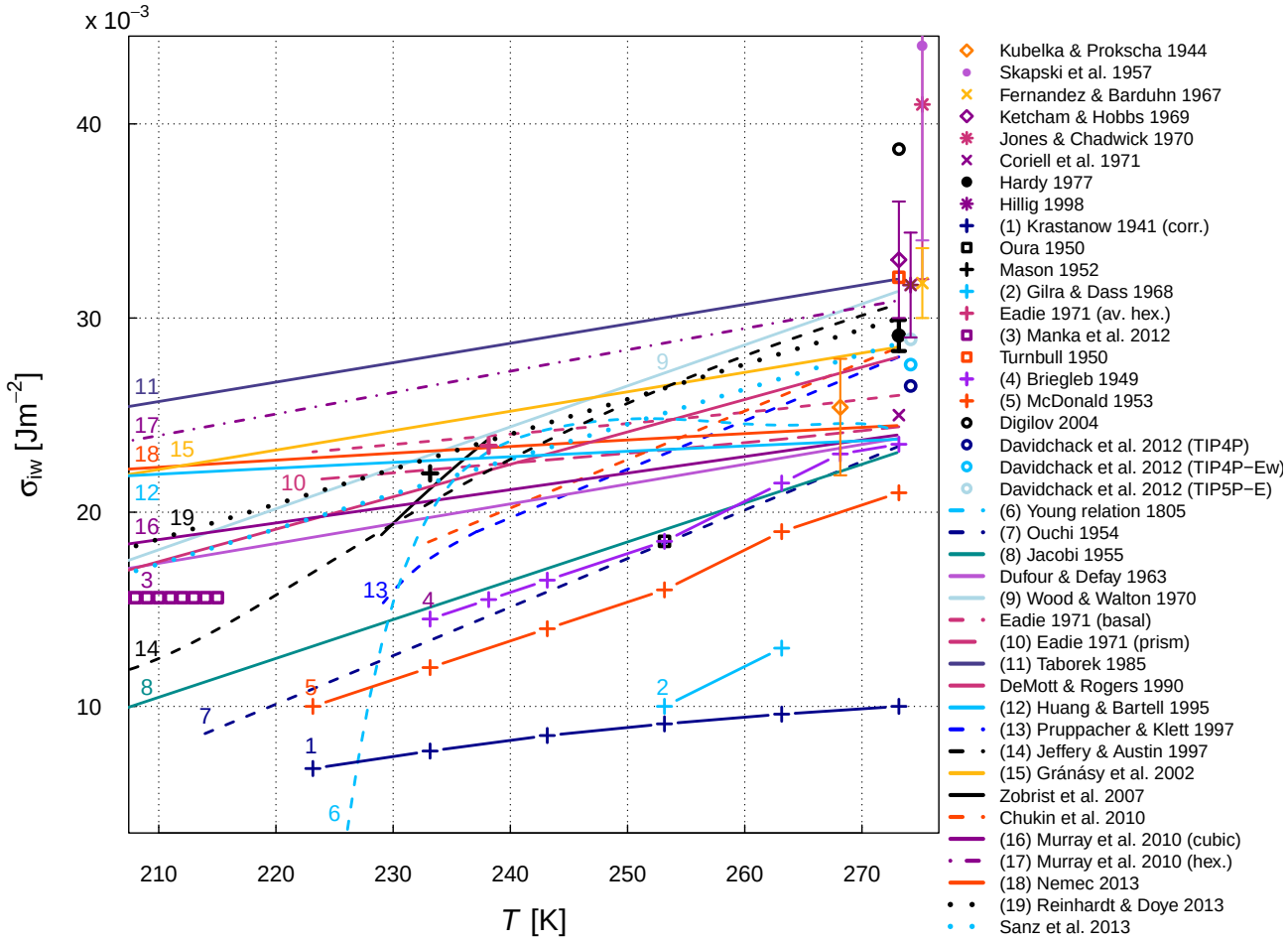

Fig. 2 Variation of the interfacial tension σ_{iw} with temperature T and measurements of σ_{iw}. Solid lines indicate estimates based on fits to nucleation measurement data, dashed lines indicate theoretical estimates, dotted lines results from molecular models. The macroscopic measurement results at the right hand side of the plot are all (besides the value of Kubelka and Prokscha [36]) measured at 273.15 K but plotted on a slightly wider temperature range to enable identification of the single points. They are shown by full circles (•), open diamonds (◇), crosses (×), and stars (∗). The error bars of the points from Skapski *et al.* [37] and Jones and Chadwick [38] are symmetric (upper limits are not shown completely). The open circled points (○) show results from molecular simulations, plus signs (+) from theoretical estimates, and open squares (□) estimates resulting from nucleation measurements.

Table 2 Summary of methods for estimating σ_{iw}

Theory	σ_{iw} based on	Dataset	Comments
Young relation 1805	equilibrium of interfacial tensions	Pruppacher & Klett 1997, Hale & Plummer 1974	
Ouchi 1954	thermodynamic concept	-	
Jacobi 1955	nucleation measurements	Jacobi 1955	
Dufour & Defay 1963	nucleation measurements	Jacobi 1955	
Wood & Walton 1970	nucleation measurements	Wood & Walton 1970	
Eadie 1971	statistical concept	-	
Taborek 1985	nucleation measurements	Taborek 1985	$\Delta g^{\#}$ constant
DeMott & Rogers 1990	nucleation measurements	DeMott & Roggers 1990	
Huang & Bartell 1995	nucleation measurements	Huang & Bartell 1995, Wood & Walton 1970, Butorin & Skripov 1972	
Pruppacher & Klett 1997	thermodynamic concept	unpublished	
Jeffery & Austin 1997	thermodynamic concept (Turnbull 1950)	-	
Gránásy et al. 2002	nucleation measurements + continuum model	Taborek 1985	
Zobrist et al. 2007	nucleation measurements	Pruppacher et al. 1998, Krämer et al. 1999, Duft and Leisner 2004, Benz et al. 2005, Stöckel et al. 2005	229 - 238 K
Chukin et al. 2010	similar as Pruppacher & Klett	-	233 - 273 K
Murray et al. 2010	nucleation measurements	Murray et al. 2010	
Němec 2013	nucleation measurements	Huang & Bartell 1995, Stan 2009, Manka et al. 2012	
Reinhardt & Doye 2013	molecular model (TIP4P)	-	
Sanz et al. 2013	TIP4P in combination with CNT	-	

σ_{iw} differs by up to a factor of three (Fig. 2) and follows differing temperature trends. It can be described in terms of two components: the magnitude of its value at the melting point ($\sigma_{iw,0}$) and its temperature dependence. Literature estimates of σ_{iw} vary between $10 \cdot 10^{-3}$ and $44 \cdot 10^{-3}$ J m^{-2} at 273.15 K, and between $6.8 \cdot 10^{-3}$ and $26.7 \cdot 10^{-3}$ J m^{-2} at 220 K. As noted above, σ_{iw} is expected to decrease with temperature. Most of the theoretical and molecular-modeling approaches suggest that this decrease should be linear, with a slope between 0.1 and $0.25 \cdot 10^{-3}$ J m^{-2} K^{-1} (see Table 3). The only studies that report a temperature dependence which is very different from a linear dependence is that of Zobrist *et al.* [29], where a function was fitted to experimental nucleation rate data without theoretical consideration, the Young relation by Pruppacher and Klett [15], where σ_{iw} was constrained by the singularity behavior of water at 228.15 K.

Describing σ_{iw} is a challenging task due to the spread of available measurement data at the melting point (see Fig. 2) and the unknown temperature behavior. In Fig. 3, the importance of the reference value $\sigma_{iw,0}$ versus the importance of the predicted temperature dependence is examined. The figure shows the temperature-dependent functions reported in the literature for a single value of $\sigma_{iw,0}$. The measured $\sigma_{iw,0}$ of Hardy [39] was taken as the reference value, in accordance with current consensus (see *e.g.* Gránásy *et al.* [40]). With an unified reference value, better agreement than Fig. 2 can be seen (narrower range of values for σ_{iw} on the ordinate). However, significant spread remains.

It is interesting to compare the results from molecular models with other estimates. The molecular-model results are fundamentally different from others, as the molecular mechanics of water molecules building clusters is explicitly simulated. Fig. 2 shows that these molecular modeling results are within the uncertainty range of Hardy [39] at 273.15 K (besides the value of Digilov, 2004). Additional information from sophisticated molecular models may be able to reduce the uncertainty in $\sigma_{iw}(T)$ in future. Nevertheless, the spread of the results reported is still quite large.

4.2 Saturation ratio

Another parameter included in the calculation of the nucleation rate is the saturation ratio [see Eq. (2)]. Murphy and Koop [42] have investigated the spread of results obtained by different parameterizations for the saturation ratio. Different formulations are in good agreement above 238.15 K, but may become significantly different at lower temperatures. Moreover the recent study of Murray *et al.* [43] shows that assuming the ice structure to be cubic instead of hexagonal changes the saturation ratio with respect to ice and σ_{iw} significantly, when estimated from nucleation measurements. Between 180 and 190 K the vapor pressure is 10.5% ± 2.5% larger for cubic ice compared to hexagonal ice. The difference gets smaller with higher temperatures (8.3% at 235 K).

The sensitivity of the nucleation rate to the calculation of the saturation vapor pressure with respect to water and ice as well as the difference between cubic and hexagonal ice is not investigated here. Most studies cited here are based on the as-

Table 3 Values from linear parameterizations of $\sigma_{iw}(T)$

Theory	$\sigma_{iw,0}$ [10^{-3} J m^{-2}]	$d\sigma_{iw}/dT$ [10^{-3} J m^{-2} K^{-1}]
Jacobi 1955	23.07 (extrapolated)	0.2
Dufour & Defay 1963	23.8 (extr.)	0.102
Wood & Walton 1970	31.93 ± 0.44 (extr.)	0.211 ± 0.012
DeMott & Rogers 1990	28	0.167
Taborek 1985	32 (extr.)	0.1
Pruppacher & Klett 1997 (237.15 K-273.15 K)	28	0.25
Gránásy et al. 2002	28.5 (extr.)	0.1
Chukin et al. 2010	28.5	0.25
Reinhardt & Doye 2013	30 (extr.)	0.18
Sanz et al. 2013	28.7	0.18

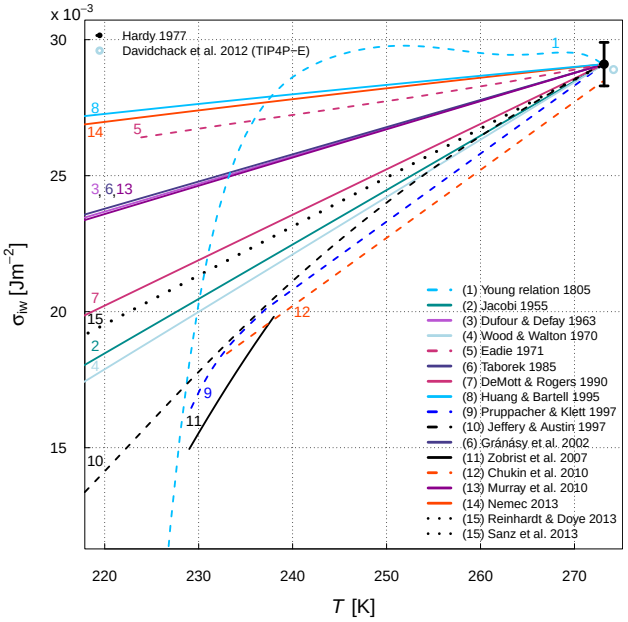

Fig. 3 Variation of the interfacial tension σ_{iw} with temperature T shifted to the measurement point of Hardy [39]. Solid lines indicate estimates based on fits to nucleation measurement data, dashed lines indicate theoretical estimates, dotted lines results from molecular models.

sumption of hexagonal ice, so that the saturation ratio was calculated for this ice type based on Goff [44] as recommended by the World Meteorological Organization [45].

5 Sensitivity analysis

In this section, the sensitivity of CNT to different parameters, parameterizations, and assumptions is analyzed by plotting the nucleation rate J_{hom} as a function of temperature. $J_{\mathrm{hom}}(T)$ is plotted for each parameter discussed in sections 3 and 4.

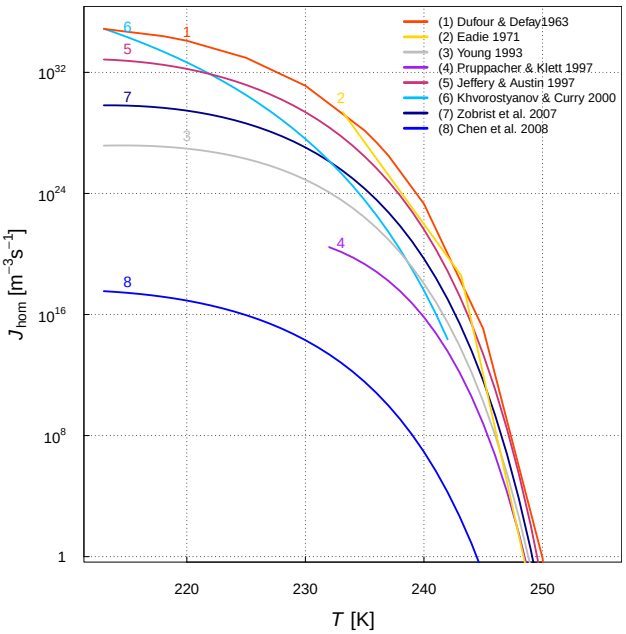

Fig. 4 Variation of the nucleation rate J_{hom} in dependence of the temperature T due to the choice of the parameterization of the activation energy $\Delta g^{\#}$. For the interfacial tension σ_{iw} the formulation of Pruppacher and Klett [15] is used (see section 4.1). The prefactor C_{prefac} was assumed to be constant (10^{41} m^{-3}s^{-1}).

Figure 4 shows that the nucleation rate J_{hom} is smaller when a high value of $\Delta g^{\#}$ is chosen, as the kinetic barrier for cluster formation thus becomes larger. Depending on the choice of $\Delta g^{\#}$, the predicted nucleation rate at 230 K differs by up to 16 orders of magnitude. This difference does not translate directly to a disagreement between the studies cited in Fig. 4, as some CNT formulations have estimated $\Delta g^{\#}$ based on other free parameters. For example, σ_{iw} has been kept the same (based on Pruppacher and Klett [15]) for all calculations in Fig. 4 but different values were originally used by the authors of those studies.

To examine the influence of the prefactor C_{prefac} on the nucleation rate, the number of water molecules in contact with the unit area of the ice germ n_{s} and the volume number density

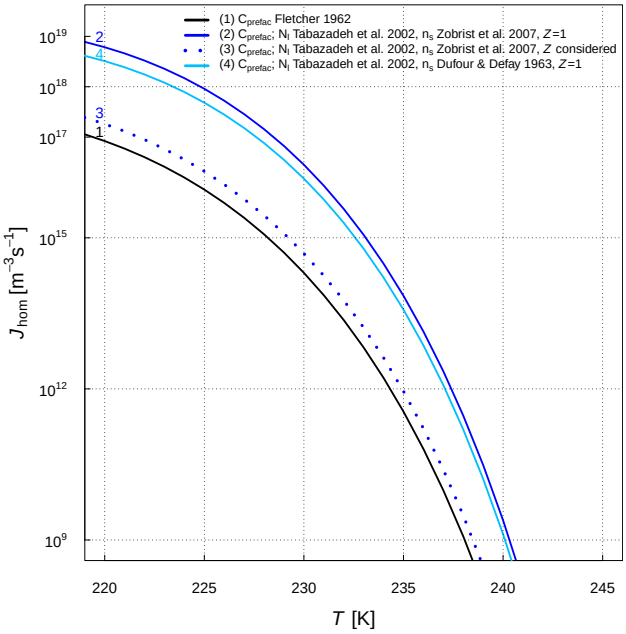

Fig. 5 Variation of the nucleation rate J_{hom} in dependence of the temperature T due to the choice of the water molecules in contact with the unit area of the ice germ n_{s} (in this case N_{l} is kept constant) and the volume number density of water molecules in liquid water N_{l} (in this case n_s is kept constant) compared to the use of an approximated total prefactor C_{prefac}. In addition the difference in taking into account the Zeldovich factor is shown. To increase the clarity of the figure only the cases with largest differences are chosen (lines which were to similar were left out). For the interfacial tension σ_{iw} the formulation of Pruppacher and Klett [15] is used (see section 4.1), the activation energy $\Delta g^{\#}$ is kept constant at $14.5 \cdot 10^{-20}$ J.

of water molecules in liquid water N_{l} were varied. Additionally importance of the Zeldovich factor was investigated. As can be seen in Fig. 5 the spread of reported literature values for n_{s} and N_{l} do not lead to a large spread in J_{hom} compared to the influence of the choice of other unconstrained parameters.

Accounting for the Zeldovich factor Z reduces the total nucleation rate in a manner dependent on the formulation used for r_{germ} [Eq. (5)] and σ_{iw}, as ΔG [Eq. (1)] and $n_{k,\mathrm{germ}}$ are part of the formula for Z [see Eq. (17)]. This dependence complicates the comparison and makes a comprehensive statement about the sensitivity of the nucleation rate caused by accounting versus non-accounting (Z=1) of the Zeldovich factor impossible. In this example, using the formulation of σ_{iw} by Pruppacher and Klett [15] lowers J_{hom} by two orders of magnitude in comparison to setting $Z = 1$.

The difference between the detailed calculation of the prefactor C_{prefac} and using an approximated temperature independent prefactor as suggested by Fletcher [11] and Young [46] is max. two orders of magnitude.

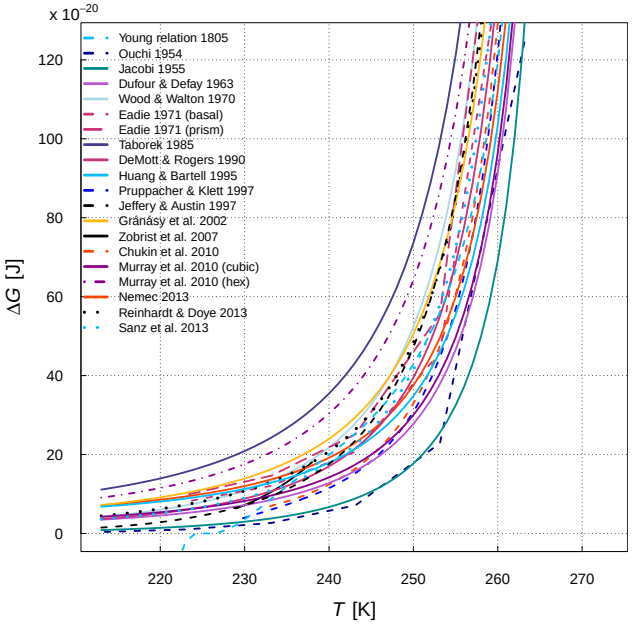

Fig. 6 Variation of the energy barrier ΔG with temperature T due to the choice of the interfacial tension σ_{iw}. Solid lines indicate estimates based on fits to nucleation measurement data, dashed lines indicate theoretical estimates, dotted lines results from molecular models.

Figure 6 shows the variation of the energy barrier ΔG due to the choice of σ_{iw}, Fig. 7 the corresponding variation in the nucleation rate. The nucleation rate can differ by around 25 orders of magnitude at 230 K (Fig. 7), which is larger than the spread due to the choice of $\Delta g^{\#}$ (16 orders of magnitude). Again, a direct comparison is difficult because there are interdependencies in the estimation of the different parameters in some studies. Therefore, Fig. 7 shows one example for a constant $\Delta g^{\#}$ based on Chen *et al.* [30] and one for $\Delta g^{\#}(T)$ based on Jeffery and Austin [3]. The spread of J_{hom} is approximately the same in both cases, providing evidence that σ_{iw} is the dominant factor controlling the shape of the curve of $J_{hom}(T)$.

The nucleation rate $J_{hom}(T)$ is governed by the exponential terms in the equation. The steepness of $J_{hom}(T)$ is dominated by the thermodynamic exponent, indicating that σ_{iw} is the controlling factor of $J_{hom}(T)$ (see Fig. 8). The kinetic exponent is more important at very low temperatures, where the energetic barrier of the freezing process becomes small enough that the process is limited by kinetics.

The sensitivity studies also show that the choice of σ_{iw} and $\Delta g^{\#}$ influences the calculated nucleation rate considerably whereas the choice of the prefacor, respectively the components of C_{prefac} does not matter so much for J_{hom}. Therefore the further focus is on σ_{iw} and $\Delta g^{\#}$ only.

Note that the spread in the nucleation rate estimates resulting from the choice of $\Delta g^{\#}$ and σ_{iw} depends on the different

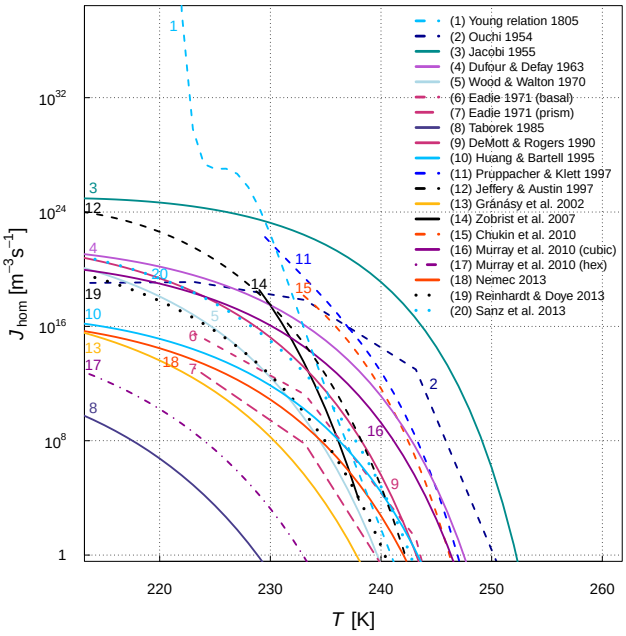

(a)

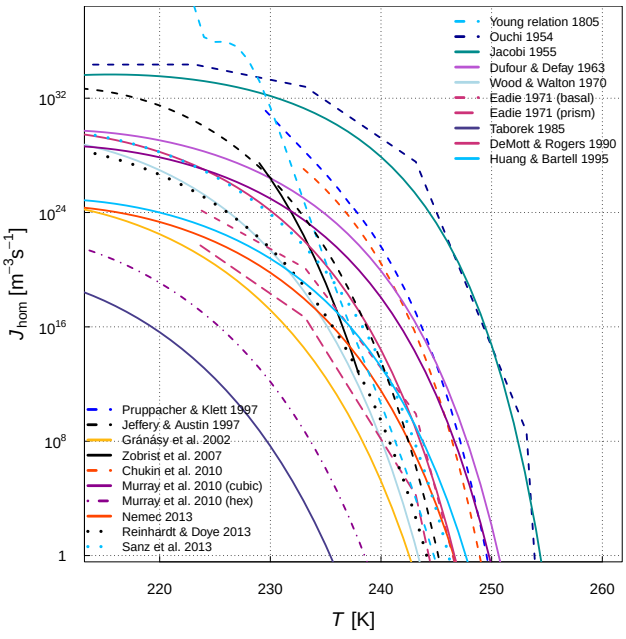

(b)

Fig. 7 Variation of the nucleation rate J_{hom} in dependence of the temperature T due to the choice of the parameterization of the interfacial tension σ_{iw} using (a) a constant activation energy $\Delta g^{\#}$ of $14.5 \cdot 10^{-20}$ J or (b) a temperature dependent activation energy $\Delta g^{\#}(T)$ based on Jeffery and Austin [3]. The prefactor C_{prefac} was assumed to be constant (10^{41} m^{-3}s^{-1}).

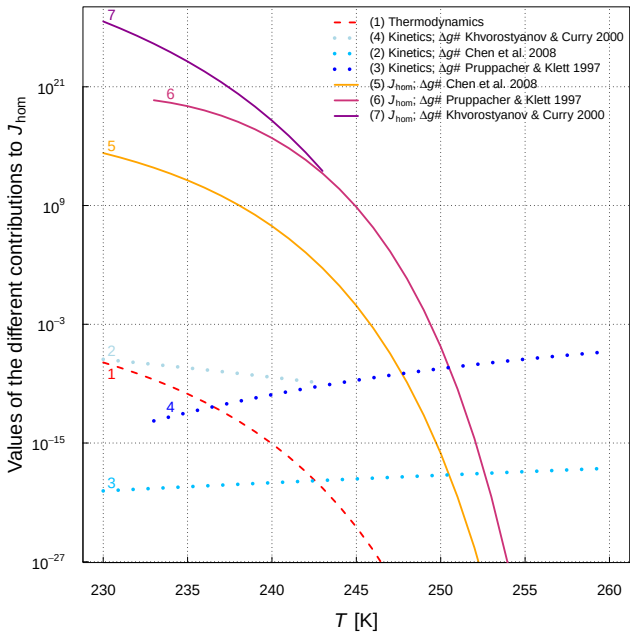

Fig. 8 $J_{\mathrm{hom}}(T)$ and the two exponential terms (thermodynamics and kinetics) of Eq. (13). The exponential terms were calculated for three different approaches of $\Delta g^{\#}$: no temperature dependence [30], increasing $\Delta g^{\#}$ with supercooling [15] and decreasing $\Delta g^{\#}$ with supercooling [20]. For the thermodynamic term the interfacial tension σ_{iw} of Pruppacher and Klett [15] was used. The prefactor C_{prefac} was assumed to be constant (10^{41} m^{-3}s^{-1}).

formulations found in literature and can not be generalized from Fig. 4 and Fig. 7. Therefore in section 5.1 the sensitivity on the parameters was investigated independent of the different formulations in the literature.

5.1 Uncertainty of using CNT

To illustrate the uncertainty resulting from the choice of the different formulations of CNT parameters, the relative error in the nucleation rate was estimated by varying the free parameters σ_{iw} and $\Delta g^{\#}$ within $\pm$ 50% from one estimate values (Fig. 9). The calculations were done at 243 K and at 233 K, as this is a temperature range around the onset of homogeneous freezing in atmospheric clouds. In Fig. 9 it can be seen that in all cases the impact of uncertainties in σ_{iw} and $\Delta g^{\#}$ is not symmetric. σ_{iw} is the parameter with the largest uncertainty (dark blue lines), which dominates the uncertainty in J_{hom}. For example at 243 K a minor decrease in σ_{iw} of 0.5% leads to an uncertainty in J_{hom} of 94%. On the other hand, decreasing $\Delta g^{\#}$ by 0.5% only changes J_{hom} by 16%. Uncertainties in σ_{iw} have a larger impact on J_{hom} than uncertainties in $\Delta g^{\#}$ at higher temperature. Note that in the case of increasing σ_{iw} or $\Delta g^{\#}$ J_{hom} decreases (towards the limit of zero) so that the relative change in J_{hom} for such an increase is always $\leq$ 100%. In that case the uncertainties approach -100%, which can not be exceeded.

Looking at the spread in the free parameters estimated by different studies in the literature, it can be seen that an uncertainty of at least 50% is common. This translates into an uncertainty in J_{hom} of 18 orders of magnitude. In contrast, measured values of J_{hom} generally differ by six orders of magnitude. A six-orders-of-magnitude uncertainty in J_{hom} translates into an uncertainty in σ_{iw} of 6% at 243 K and 18% at 233 K, and in an uncertainty in $\Delta g^{\#}$ of 35% for the whole temperature range. Note that the temperature dependence of the uncertainty due to variation of $\Delta g^{\#}$ is negligible here. With this level of precision, it is not possible to decide which literature formulation of σ_{iw} and $\Delta g^{\#}$ is the most realistic. Nevertheless in the next section we try to constrain possible ranges for σ_{iw} and $\Delta g^{\#}$ from a fitted function of J_{hom}.

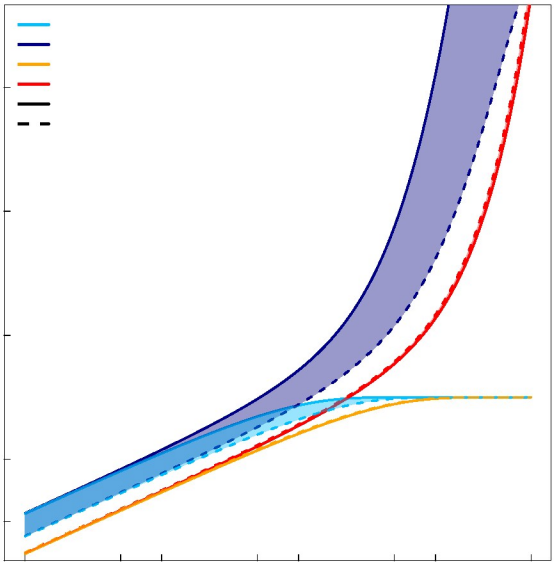

(a)

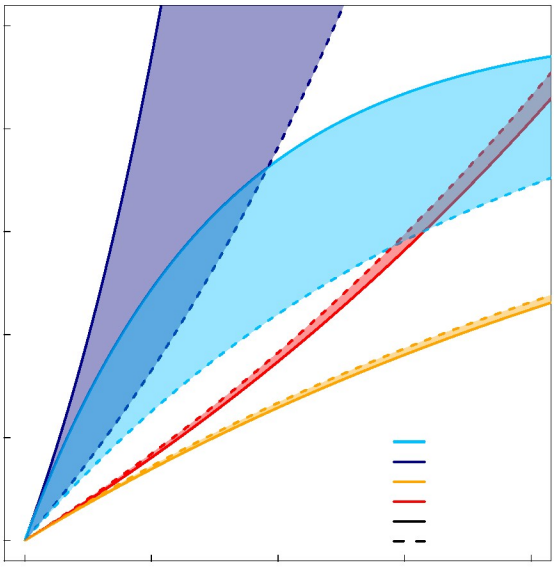

(b)

Fig. 9 Magnitude of deviation from a reference ice nucleation rate J_{hom} in percent (relative uncertainty). The results are shown for a variation of the values of σ_{iw} and $\Delta g^{\#}$ from (a) 0.01 to 50% in the temperature range of 233 to 243 K (shaded area) and (b) for a variation of 0 to 2% (zoom of (a)).

6 Constraining σ_{iw} and $\Delta g^{\#}$ with J_{hom}

The sensitivity analysis of section 5 shows that it is difficult to evaluate the formulations of $\Delta g^{\#}$ and σ_{iw} separately. Additionally, many authors fix one of the parameters (based on theoretical considerations), while the other one is then estimated by fitting plausible freezing rates to experimental data. The choice of the fit parameter influences the values of the other free parameters. Therefore an estimate of the nucleation rate $J_{\mathrm{hom}}(T)$ will be used here to express $\Delta g^{\#}$ or σ_{iw} depending on the different theoretical formulations (see Appendix A and C) of either σ_{iw} or $\Delta g^{\#}$. By using the whole range of approaches and assumptions, the range of the free parameters can be constrained within the uncertainty limits of $J_{\mathrm{hom}}(T)$. From this analysis a suitable temperature dependence emerges. Moreover all possible combinations of the different theoretical formulations of σ_{iw} and $\Delta g^{\#}$ are explored by using the fit result to appoint the best combination.

6.1 Fitting J_{hom} to experimental data

A comprehensive dataset of 33 homogeneous freezing measurements was collected and fitted by least-squares minimization using three different approaches, which are explained further on. The dataset consists of measurements from many different experimental setups collected over the last few decades, covering different temperature ranges. An overview of the dataset and the used measurement techniques can be found in chronological order in Table 4 and in Figs. 10 and 11. Table 4 includes information about the temperature uncertainty of the measurement. In Figs. 10 and 11 the measurement uncertainty of the nucleation rate can be seen. Note that the measurement uncertainty of the nucleation rate does not reflect the uncertainty introduced by experimental parameters, which has been discussed in Riechers *et al.* [47]. The raw data would be needed to be able to re-evaluate the measurements and evaluate uncertainties. The re-evaluation of the data is beyond the scope of this paper, but important for any future analysis (see section 7). On the premise that measurement techniques have got more precise over the years, the dataset was divided almost equally into measurements made before or after the year 2000 (indicated by red and blue colors in Fig. 10 and Fig. 11). Note that the data from Huang and Bartell [6], Bartell and Chushak [48] and Manka *et al.* [49] were not measured at atmospheric pressure but at high pressure conditions due to the use of supersonic nozzles. The data were nevertheless included to guide the fitting algorithm in the low temperature regime. In addition to the 33 measurements, the simulated nucleation rates from Sanz *et al.* [50] were added to guide the fit in the high-temperature regime (see Table 4).

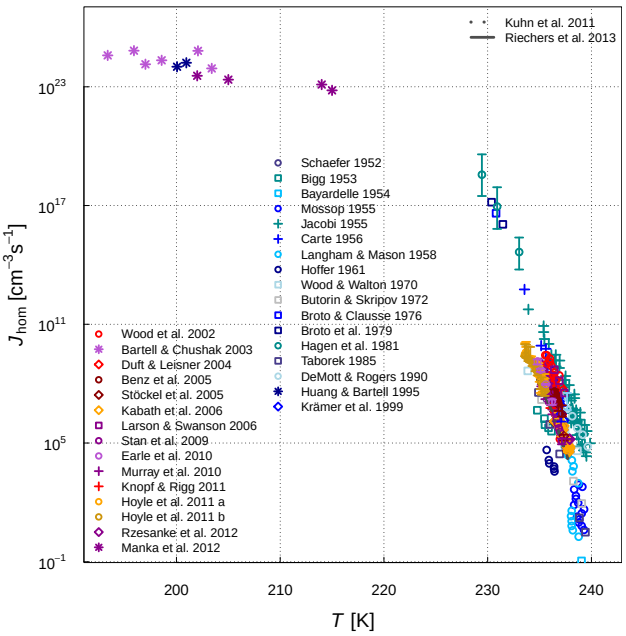

Fig. 10 Homogeneous freezing measured by several authors. A list of all datasets taken into account including the measurement method and the temperature uncertainty can be found in Table 4 (horizontal error bars were omitted on account of clarity). Blue colors characterize measurements done before the year 2000, red colors characterize measurements done after the year 2000. The symbols indicate the measurement method: open circled points (○) Cloud and aerosol chamber experiments (droplet in air); plus signs (+) Cold stage experiments (droplet on a solid plate); open squares (□) Suspension, emulsion and dispersion experiments (droplet in liquid); open diamonds (◇) Levitated drop in electrodynamic balance; stars (∗) Electron diffraction.

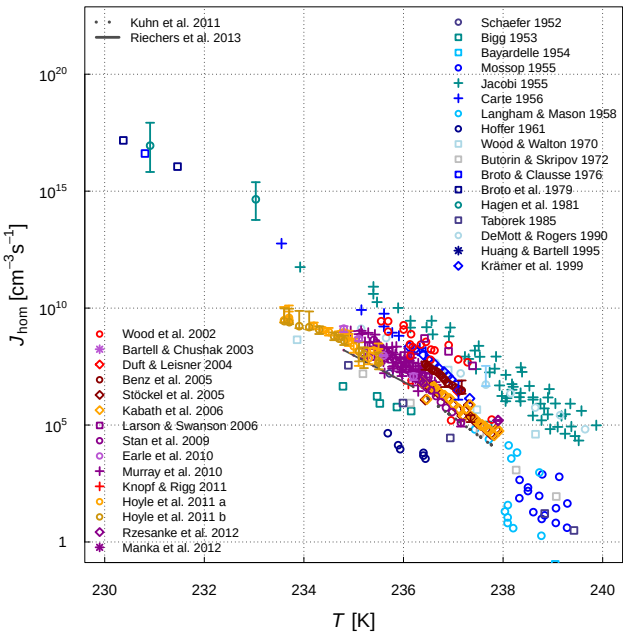

Fig. 11 Same as Figure 10 but showing a limited temperature range.

To estimate the nucleation rate $J_{\mathrm{hom}}(T)$ the dataset was fitted following a CNT formulation equivalent to Eq. (13). A constant prefactor C_{prefac} of $10^{41}\,\mathrm{m}^{-3}\mathrm{s}^{-1}$, a constant activation energy $\Delta g^{\#}$, and a linear T-dependent σ_{iw} with the reference value $\sigma_{\mathrm{iw},0}$ of Hardy [39] was used:

$$J_{\mathrm{hom}} = C_{\mathrm{prefac}} \cdot \exp\left(-\frac{\Delta g^{\#}}{k_{\mathrm{B}}T}\right) \cdot \exp\left(-\frac{16\pi \cdot v_{\mathrm{ice}}^2 \cdot (29.1 + d\sigma_{\mathrm{iw}}/dT \cdot T_{\mathrm{c}})^3}{3(k_{\mathrm{B}}T)^3 \ln(S_{\mathrm{i}})^2}\right) \quad (18)$$

The fit parameters are thus the slope of $\sigma_{\mathrm{iw}}(T)$ ($d\sigma_{\mathrm{iw}}/dT$, fit parameter A) and $\Delta g^{\#}$ (fit parameter B).

In a first step, the fit was done by combining all measurements into one large dataset to investigate the general behavior of the fitting formula. It can be seen in Fig. 12 that a reasonable good fit was possible. However, the fitted $\Delta g^{\#}$ is negative, which translates into a missing activation energy barrier for the nucleation process and therefore does not seem to be reasonable. As the fit is biased by the number of data in each dataset, a weighting function for each measurement value, which is the reciprocal of the number of data in the corresponding dataset, was next introduced giving all datasets equal weight. This may have introduced problems, as the quality of each dataset is different. However, not enough information is available to decide which datasets should or should not be taken into account. A physically-meaningful weighting would be the temperature uncertainty of the measurement, as this strongly affects these results [47]. Unfortunately this information was not available for quite a few datasets.

Looking at the whole spectrum of measurements in Fig. 10, differences in the slope of the data between datasets can be seen. To take such differences into account, a grouped-data object was created out of the individual datasets. With this method, information about the grouping of the data is not lost. The grouping factor is the measurement method and the time of publication. This procedure splits the dataset into several datasets which are fitted separately. An advantage of this method is that the resulting fit parameters of the individual fits can be compared to check whether the parameters vary among individual datasets. The correlation between the two fit parameters can also be tested. A disadvantage of this method is that small datasets (containing less than three values) have to be excluded. Therefore, the dataset of Broto *et al.* [63] and Broto and Clausse [64] were combined to one dataset, as well as the dataset of Huang and Bartell [6] and Bartell and Chushak [48]. The datasets of Knopf *et al.* [65], Duft and Leisner [66], Rzesanke

et al.[67], Bayardelle[68] and Schaefer[69] were omitted because they are too small and could not be reasonably combined with other datasets.

To take into account the individual characteristics of each dataset, we estimate fixed and random effects for the grouped-data object using a non-linear mixed-effect model[70,71]. The fixed effects represent the value of the fit parameter throughout all datasets, the random effects the variation in the fit parameter between the individual datasets. The amount of random effects needed can be estimated from the intervals of the fit parameters for the individual datasets resulting from the fit of the grouped data object. Figure 13 shows the intervals of the fit parameters for all datasets. The results are sorted by J-values (starting with highest nucleation rates). No trend is seen with time (origin of dataset) and/or measurement method.

The fitted parameters differed from dataset to dataset but were correlated (Fig. 14). This correlation underlines the earlier statement that the choice of one free parameter influences the other one. Note that because of this correlation, uncertainties of one quantity can be compensated by the other one.
A simplified mixed-effect model was created based on these results. Only the slope of σ_{iw} was taken as a fit parameter, having fixed and random effects, while $\Delta g^{\#}$ obtained from the fit of the weighted dataset was used. The results of the different fitting methods can be found in Table 5 and seen in Fig. 15. This mixed-effect model, which is statistically the best solution, was used for the further analysis.

Note that using a trustful reference dataset for $J_{\mathrm{hom}}(T)$ instead of using the whole comprehensive dataset from all peer-reviewed articles could improve the analysis (see section 7).

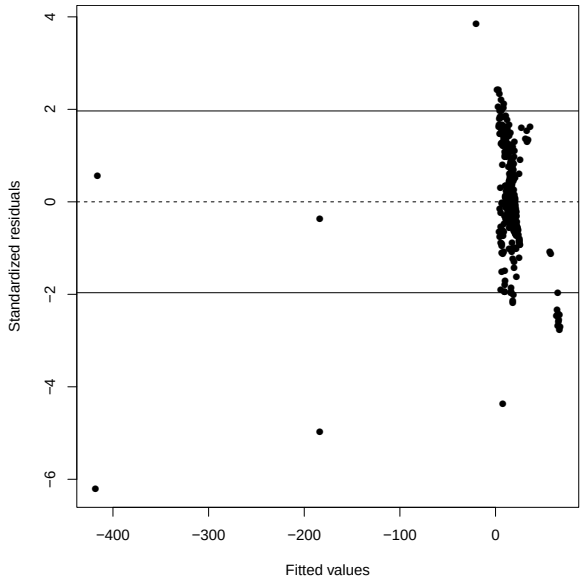

(a)

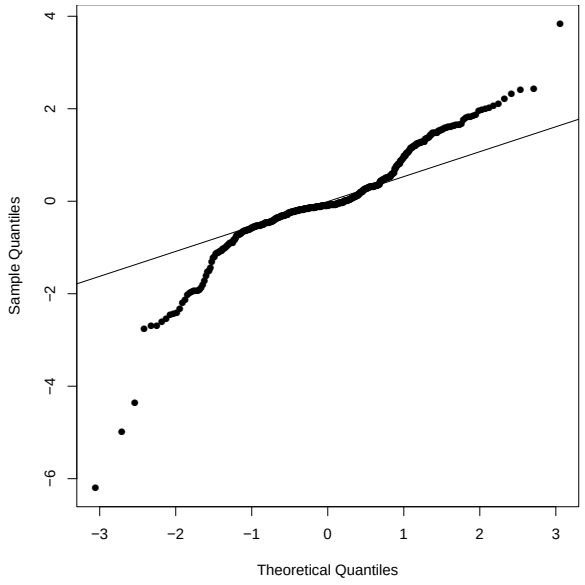

(b)

Fig. 12 Statistics of the fitting formula [Eq. (18)] for fitting the collected dataset of homogeneous freezing data (see orange curve in Fig. 15). Figure (a) shows the standardized residuals plotted against the values of $\ln(J)$. Figure (b) shows the normal q-q plot of the standardized residuals, where the quantiles of the standardized residuals are plotted against the theoretical quantiles from a normal distribution.

Table 4 Dataset of measurements of the homogeneous freezing rate J_{hom} (sorted chronologically; 1952-2013); DSC stands for Differential scanning caliometry, EDB for Leviated drops in electrodynamic balance.

#	Dataset	Measurement technique	Uncertainty range (T)	Comments
1	Schaefer 1952	Cloud chamber	± 0.5 K	
2	Bigg 1953	Suspension	± 0.5 K	two immiscible liquids
3	Bayardelle 1954	Suspension	-	mercury and silicone
4	Mossop 1955	Cloud chamber	± 0.2 K	
5	Jacobi 1955	Cold stage	± 0.2 K	
6	Carte 1956	Cold stage	± 0.6 K	silicone oil
7,8	Langham & Mason 1958	Cloud chamber	-	
9	Hoffer 1961	Cloud chamber	± 0.5 K	droplets in silicone oil
10	Wood & Walton 1970	Emulsion	± 0.1 K	water and oil; significant variation from run to run
11	Butorin & Skripov 1972	DSC	-	
12a	Broto & Clausse 1976	DSC	± 0.5 K	
12b	Broto et al. 1979	DSC	± 0.5 K	
13	Hagen et al. 1981	Cloud chamber	-	very fast droplet growth → droplet size, T from droplet growth model
14	Taborek 1985	DSC	-	water and petroleum
15	DeMott & Roggers 1990	Cloud chamber	± 0.2 K	no direct optical detection → settling time correction
16a	Huang & Bartell 1995	Electron diffraction	T not measured	at pressures of 4.4 bar → J may be altered; very fast nucleation → droplet growth model
17	Krämer et al. 1999	EDB	± 0.1 K	
18	Wood et al. 2002	Cloud chamber	± 0.2 K	
16b	Bartell & Chushak 2003	Electron diffraction	T not measured	
19	Duft & Leisner 2004	EDB	± 0.002 K	
20	Benz et al. 2005	Cloud chamber	± 0.3 K	Exp. Nr. 2
21	Stöckel et al. 2005	EDB	± 0.25 K	
22	Kabath et al. 2006	EDB	-	
23	Larson & Swanson 2006	Emulsion	± 0.5 K	
24	Stan et al. 2009	Emulsion	± 0.4 K	
25	Earle et al. 2010	Cloud chamber	± 0.5 K	
26	Murray et al. 2010	Cold stage	$< \pm$ 0.6 K	
27	Knopf & Rigg 2011	Cold stage	± 0.15 K	
28,29	Hoyle et al. 2011	Cloud chamber	± 0.4 K	30/a) 800 nm droplets 31/b) 200 nm
30	Kuhn et al. 2011	Cloud chamber	± 0.5 K	
31	Rzesanke et al. 2012	EDB	± 0.1 K	
32	Manka et al. 2012	Vibration spectroscopy	-	
33	Riechers et al. 2013	Emulsion	± 0.3 K	water and oil
(34)	Sanz et al. 2013	TIP4P	-	simulation results
(35)	Sanz et al. 2013	TIP4P/Ice	-	simulation results

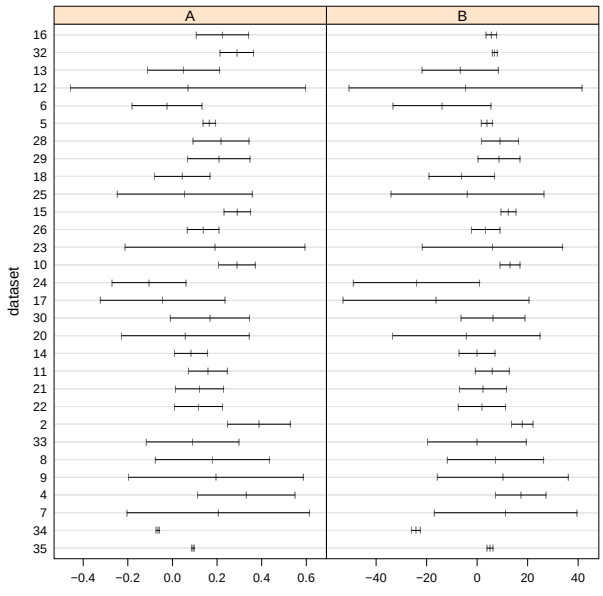

Fig. 13 Results of the fitting parameters A and B from fitting the grouped data object of J_{hom}, sorted by J-values (starting with highest nucleation rates). Each line (y-axis) stands for one dataset labeled by the corresponding number (see Table 4) with the fitting parameter on the x-axis.

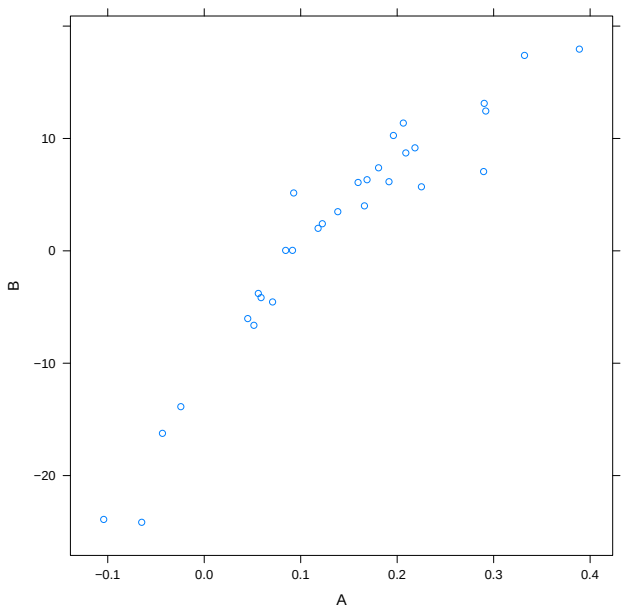

Fig. 14 Correlation of the two fitting parameters A and B. The fitting parameter B (y-axis) is plotted against the fitting parameter A (x-axis).

Table 5 Results of fitting measurement dataset of J_{hom}

Fitting method	Fit parameter	Standard deviation
Fit 1	$A = d\sigma_{\mathrm{iw}}/dT = 0.046094\ \mathrm{J\ m^{-2}\ K^{-1}}$	$5.155{\cdot}10^{-3}\ \mathrm{J\ m^{-2}\ K^{-1}}$
	$B = \Delta g^{\#} = -5.062232 \cdot 10^{-20}\ \mathrm{J}$	$0.545589 \cdot 10^{-20}\ \mathrm{J}$
Fit 2; weighted dataset	$A = 0.130857\ \mathrm{J\ m^{-2}\ K^{-1}}$	$9.023 \cdot 10^{-3}\ \mathrm{J\ m^{-2}\ K^{-1}}$
	$B = 2.591893 \cdot 10^{-20}\ \mathrm{J}$	$0.746252 \cdot 10^{-20}\ \mathrm{J}$
Fit 3; mixed-effect model	$A = 0.1240907\ \mathrm{J\ m^{-2}\ K^{-1}}$	$0.003925824\ \mathrm{J\ m^{-2}\ K^{-1}}$
	$B = 2.591893 \cdot 10^{-20}\ \mathrm{J}$	fixed

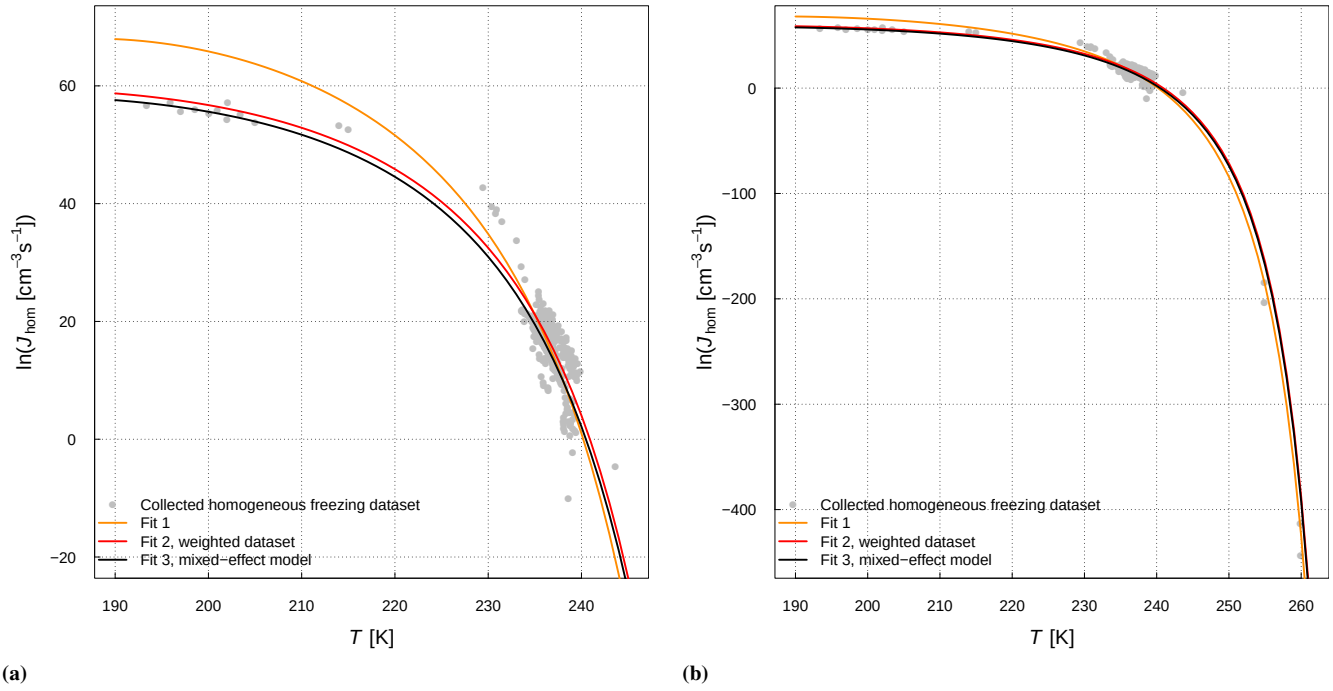

Fig. 15 Fitting results for $J_{\mathrm{hom}}(T)$ from (a) 190 K - 240 K and (b) 190 K - 260 K compared to the collected homogeneous freezing dataset.

6.2 Constraining σ_{iw} and $\Delta g^{\#}$ using the fit of $J_{hom}(T)$

The final fit to J_{hom} (mixed-effect model) obtained in section 6.1 gives a picture of the nucleation rate over a wide temperature range. Moreover, the fitted $J_{hom}(T)$ can be used to better constrain the values of σ_{iw} and $\Delta g^{\#}$ found in literature. In the discussion that follows, the fitted $J_{hom}(T)$ was used 1.) to constrain a reasonable range and behavior of σ_{iw} and $\Delta g^{\#}$, and 2.) to evaluate different literature formulations of $\Delta g^{\#}$ and σ_{iw}.

1. **Constraints on σ_{iw} and $\Delta g^{\#}$ from $J_{hom}(T)$**

   If $J_{hom}(T)$ and C_{prefac} is known, according to Eq. (13), one of σ_{iw} or $\Delta g^{\#}$ can be evaluated based on the other. For example, the fitted $J_{hom}(T)$ can be used to predict σ_{iw} using different literature formulations for $\Delta g^{\#}$ (some of which are independent of σ_{iw} with the exception of the constant approach from Chen *et al.* [30]). The results may be evaluated in terms of their temperature dependence and plausibility.

   Figure 16 shows the fitted nucleation rate $J_{hom}(T)$ for different temperatures (colored lines) as a function of the two parameters $\Delta g^{\#}$ and σ_{iw}.The black symbols represent different estimates for $\Delta g^{\#}$ (a) or σ_{iw} (b) as proposed by various authors. These estimates are all independent of σ_{iw} (a) or $\Delta g^{\#}$ (b). For each estimated $\Delta g^{\#}$ or σ_{iw}, σ_{iw} or $\Delta g^{\#}$ is constrained by $J_{hom}(T)$ as following a different functional form, as shown by the black lines in Fig. 16.

   A linear dependence of σ_{iw} on temperature (as expected; Section 4.1) implies that the black lines in Fig. 16(a) should be curved, which can also be seen in Fig. 16(b). Where this is not the case, σ_{iw} is only linear for low temperatures at low $\Delta g^{\#}$ where the isolines of $J_{hom}(T)$ are nearly equidistant. Other formulations of $\Delta g^{\#}$, which lead to a non-linear temperature dependence of σ_{iw} (*e.g.* the one of Chen *et al.* [30]), may be interpreted as being inconsistent with theoretical expectations.

   The temperature trend in σ_{iw} given by the formulation of Pruppacher and Klett [15] suggests that σ_{iw} becomes negative at temperatures below 223 K, which reflects a transition to unstable conditions, where no thermodynamic equilibrium exists. The temperature dependence of $\Delta g^{\#}(T)$ would need to reverse below this temperature, if σ_{iw} is to decrease with T but has a positive value. On the other hand, the $\Delta g^{\#}$ formulation of Jeffery and Austin [3] leads to reasonable values of σ_{iw} over the whole temperature range.

   As shown by the steepness of the J_{hom} curves in Fig. 16 for temperatures above 233 K, σ_{iw} is not strongly influenced by the temperature dependence of $\Delta g^{\#}$. For these temperatures, $\Delta g^{\#}$ could therefore be approximated as a temperature-independent constant. In contrast, the value of $\Delta g^{\#}$ becomes increasingly important for lower temperatures. As the size of an ice germ decreases with temperature, it is possible that the capillary assumption (Section 2.1) may not hold at these low temperatures.

2. **Evaluation of different formulations of σ_{iw} and $\Delta g^{\#}$**

   Different formulations of $\Delta g^{\#}$ and σ_{iw} were collected from literature and evaluated against the fitted $J_{hom}(T)$. The selected formulas are independent of one another (the formulations based on theoretical concepts were chosen) with the exception of the Chen *et al.* [30]-formulation of $\Delta g^{\#}$, which has been included to see how a temperature independent formulation of $\Delta g^{\#}$ behaves. Nucleation rates $J_{hom}(T)$ were calculated using these formulations [Eq. (13)] and the difference between these calculated rates and the fitted $J_{hom}(T)$ was evaluated for the atmospherically-relevant temperature range 230-250 K based on the relative uncertainty at 223 K, 233 K, 243 K and 253 K (Fig. 17).

   We find that the formulation of $\Delta g^{\#}$ is of secondary importance between 230 and 250 K. Moreover, while some formulations show good agreement with the fit until 245 K, very few formulations also show good agreement at lower temperatures. The combination of the σ_{iw} formulation of Reinhardt and Doye [72], which is based on molecular model simulations, and the $\Delta g^{\#}$ formulation of Zobrist *et al.* [29], which is based on self-diffusivity measurements, leads to the best agreement with our $J_{hom}(T)$. The resulting curve is shown with the fit and the homogeneous dataset in Fig. 17. Besides in Fig. 16(a) it can be seen that both curves lie on top of each other or at least close in this temperature range. However, for low temperatures the combination of both parameters does not give a nucleation rate close to the fitting result (the curves in 16(a) deviate from each other).
   Note that this result is self-consistent but has to be used with caution since it is dependent on $J_{hom}(T)$ and the formulations of σ_{iw} and $\Delta g^{\#}$ used in the analysis.

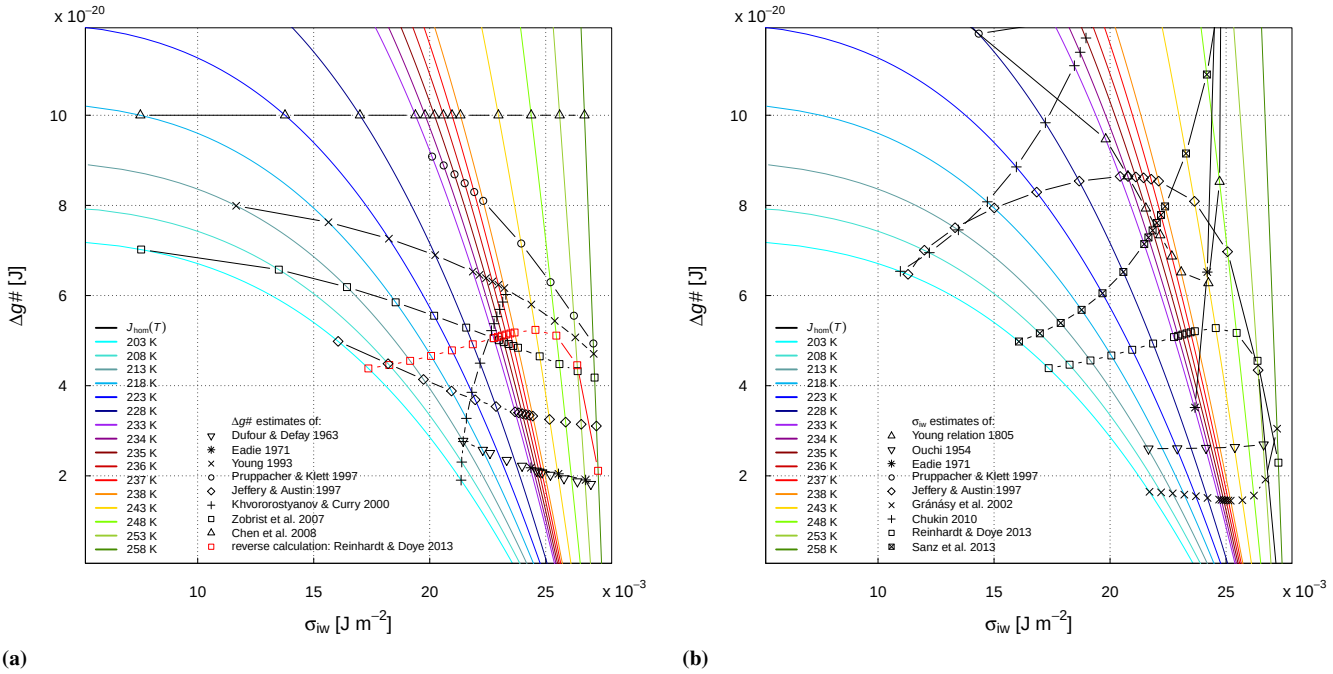

Fig. 16 Plausible combinations of σ_{iw} and $\Delta g^{\#}$ reproducing J_{hom} in the temperature range from 203 K - 258 K (colored lines). (a) Different literature estimates of $\Delta g^{\#}$ together with the matching σ_{iw} are shown in black. The reverse calculation of Reinhardt and Doye [72] is shown in red meaning the matching $\Delta g^{\#}$ for their estimate of σ_{iw}. (b) Different literature estimates of σ_{iw} together with the matching $\Delta g^{\#}$ are shown in red.

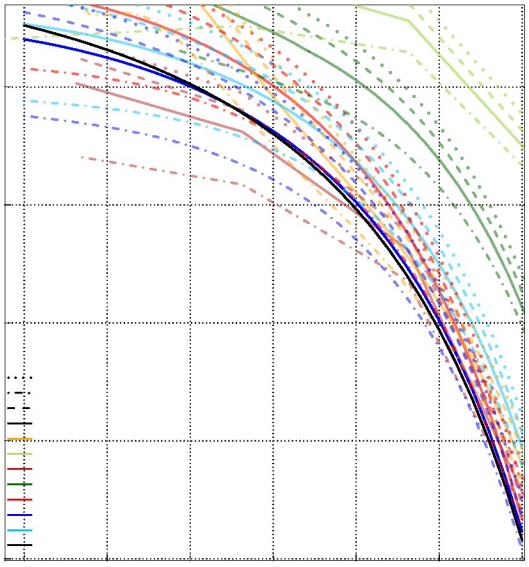

Fig. 17 Comparison of the fitted $J_{\mathrm{hom}}(T)$ (solid black line) with calculated nucleation rates using different formulations of σ_{iw} and $\Delta g^{\#}$. All lines besides the fitted $J_{\mathrm{hom}}(T)$ (solid black line) and the best-fitting combination of σ_{iw} and $\Delta g^{\#}$ (solid blue line) are made transparent to increase clarity.

7 Conclusions and outlook

Due to a poor understanding of the physics of supercooled water, the theory of CNT is poorly constrained. Key thermodynamic and kinetic parameters in the theory remain to be understood. Multiple studies have attempted to define these parameters, using different methods which have resulted in diverse findings. Consequently, multiple different formulations of CNT exist. Depending on the formulation used, CNT-predicted ice nucleation rates may differ widely. This difference contributes significantly to uncertainties in regional and global climate models when CNT-based freezing parameterizations are used.

This study gives an overview of the different thermodynamic and kinetic parameters in CNT. The physical considerations or assumptions which these parameters are based on are summarized, and the uncertainties associated with the choice of their different formulations are discussed. It is concluded that CNT is most sensitive to the interfacial tension between ice and water, σ_{iw}. Uncertainties in σ_{iw} dominate uncertainties in the nucleation rate J_{hom}. While measurements of J_{hom} differ by six orders of magnitude at 230 K, predicted values of J_{hom} can differ by 25 orders of magnitude for the different formulations of σ_{iw} in the literature. To reconcile these differences, σ_{iw} needs to be known to within 10% accuracy.

To better constrain the two most important free parameters of CNT, σ_{iw} and $\Delta g^{\#}$, we fitted measured homogeneous nucleation rates from 33 droplet-freezing experiments which used a variety of experimental techniques. Based on the resulting function $J_{\mathrm{hom}}(T)$ and on literature formulations for the activation energy $\Delta g^{\#}$, respectively σ_{iw}, we calculated σ_{iw}, respectively $\Delta g^{\#}$, and compared it with literature results. From this analysis it emerged that either σ_{iw} is thermodynamically undefined at low ($\approx < 230$ K) temperatures, or the temperature dependence of $\Delta g^{\#}$ reverses at these temperatures. Further studies are needed to evaluate these possibilities. However, for atmospheric applications, these issues arise outside of the relevant temperature range (but might be important for other fields). Thus it can be concluded that $\Delta g^{\#}$ can be set to a temperature-independent constant to simplify CNT formulations of atmospheric homogeneous freezing.

Different literature formulations of σ_{iw} and $\Delta g^{\#}$ were also evaluated for consistency with the fitted J_{hom} in the temperature range 230 K $< T <$ 250 K. It was found that the σ_{iw} formulation of Reinhardt and Doye [72] in combination with the $\Delta g^{\#}$ formulation of Zobrist *et al.* [29] performed best within the framework of this analysis.

Four major issues with regard to constraining CNT remain. First, better measurements or estimates of σ_{iw} at the melting point would better constrain $\sigma_{\mathrm{iw}}(T)$ for supercooled water. Modern experimental techniques or molecular modeling may be helpful. Second, the behavior and definition of σ_{iw} at low temperatures and third, the behavior of $\Delta g^{\#}$ at these temperatures remains poorly understood. The fourth issue is the nucleation rate itself- reducing the spread in nucleation rate measurements and thus decreasing uncertainty helps to better constrain the free parameters of CNT. This could be done by agreed guidelines for the definition of the experimental parameters and improved experimental control and awareness of uncertainties of T,V_{drop} and t. Using such guidelines enables a re-evaluation of the homogeneous freezing datasets to create a trustful reference dataset for $J_{\mathrm{hom}}(T)$.

Note that, because CNT is not a fully constrained theory yet, it would be helpful to specify which formulation and estimates of the free parameters are used when applying CNT to predict nucleation rates or interpret data.

A Methods for estimating $\Delta g^{\#}$

- Dufour and Defay [12]:

  In Dufour and Defay $\Delta g^{\#}$ is calculated by using the viscosity of water η [see Eq. (14)] leading to:

  $$\Delta g^{\#}[\mathrm{J}] = k_\mathrm{B} \cdot T \cdot \ln\left(\frac{v_{\mathrm{H_2O}} \cdot \eta}{h \cdot N_\mathrm{A}}\right) . \quad (19)$$

  For Fig. 1 the formulation of Huber *et al.* [73] is used to calculate the viscosity of water η (originally η was based on Dorsey, 1940).

- Eadie [7]:

  Unlike in other publications, the activation energy is estimated based on the dielectric relaxation time of water (τ). For this purpose the measurement of Collie *et al.* [75] is used and interpolated with a four-point Newton interpolation, which leads to similar results as in Dufour and Defay [12]. An advantage of this method can be seen in Eq. (16)- different from the other methods there is no offset value (τ_0) which has to be estimated first.

- Young [13]:

  In Young $\Delta g^{\#}$ is defined as the energy needed to break one hydrogen bond. This energy is estimated based on measurements of the viscosity of supercooled water using a capillary flow technique by Hallett [76] and on measurements of the nucleation process in a cloud chamber at 233.15 K by Hagen *et al.* [5] leading to:

  $$\Delta g^{\#}[\mathrm{J}] = 3.6 \cdot 10^{-20} - 7.3 \cdot 10^{-22} \cdot T_\mathrm{c} \quad (20)$$

  with T_c the temperature in °C. This formulation is also used by Chukin *et al.* [77].

- Pruppacher and Klett [15]:

  In Pruppacher and Klett $\Delta g^{\#}$ is estimated from a fit to laboratory data of the self-diffusion coefficient of water. For this the following measurements were used: in the temperature range between 273.15 K and 318.15 K the data based on a diaphragm-cell technique by Mills [78] and the evaluation of Mills [79], where existing measurement data has been listed and reviewed. In the temperature range of supercooled water the data of Gillen *et al.* [80] and Pruppacher [81] were used. Gillen *et al.* [80] used a fixed gradient spin-echo nuclear magnetic resonance (NMR) method to measure the self-diffusivity between 298.15 K and 242.15 K. Pruppacher [81] did measurements of the self-diffusivity of water in the temperature range of 303.15 K to 248 K. To estimate $\Delta g^{\#}$ from self-diffusivity measurements an effective activation energy was defined:

  $$\Delta g^{\#} = -R \cdot d(\ln D)/d(T^{-1}) , \quad (21)$$

  resulting in the following cubic fit of the activation energy:

  $$\Delta g^{\#}[\mathrm{J}] = a_0 \cdot \exp(a_1 T_\mathrm{c} + a_2 T_\mathrm{c}^2 + a_3 T_\mathrm{c}^3) , \quad (22)$$

  with a_0 = 5.55 · 4184/(6.022 · 10^{23}) J, a_1 = -8.423 · 10^{-3}, a_2 = 6.384 · 10^{-4} and a_3 = 7.891 · 10^{-6}, which is valid in the temperature range from 310.15 to 233.15 K [Pruppacher and Klett, 2000; Eq. (3.22)].

  The method has the disadvantage of implicitly assuming that the temperature dependence of $\Delta g^{\#}$ is weak compared to the $1/T$-dependence of the exponential in Eq. (15), which may not be true for supercooled water [3].

- Jeffery and Austin [3]:

  Jeffery and Austin used measurements of the self-diffusion of water from Prielmeier *et al.* [82] and Harris and Woolf [83] to estimate $\Delta g^{\#}$. The data from Prielmeier *et al.* [82] was used to fit the temperature dependence with the Vogel-Fulcher-Tammann (VFT) approach. D_0 was estimated from the data of Harris and Wolf, resulting in:

  $$\Delta g^{\#}[\mathrm{J}] = RT \cdot \left(\frac{B}{T - T^*} - \ln\left(\frac{D^*}{D_0}\right)\right) \quad (23)$$

  with $B = 347\ \mathrm{K}^{-1}$, $T^* = 177$ K, $D^* = 4.14 \cdot 10^{10}\ \mathrm{m^2 s^{-1}}$ and $D_0 = 349 \cdot 10^{10}\ \mathrm{m^2 s^{-1}}$.

- Khvorostyanov and Sassen [19]/Khvorostyanov and Curry [20]:

  Khvorostyanov and Sassen discuss an extension to the Pruppacher and Klett [15] formulation. $\Delta g^{\#}$ for low temperatures ($T < 243.15$ K) is described as the activation energy across the liquid-ice boundary taking into account enhanced cooperation of molecules when transferring into the ice lattice at low temperatures. Therefore the sign of $d\Delta g^{\#}/dT$ is different to all other formulations giving a negative temperature-depended relation ($\Delta g^{\#}$ is decreasing with decreasing T). The parameterization is based on fitted values for homogeneous freezing at $T < 243.15$ K following Jensen *et al.* [84]. Fitting the nucleation rate with the Pruppacher and Klett [15] formulation of σ_iw results in an activation energy of the following form:

  $$\Delta g^{\#}[\mathrm{J}] = 0.694 \cdot 10^{-12} \cdot (1 + 0.027 \cdot (T_\mathrm{c} + 30)) . \quad (24)$$

  Because this equation can give negative values, it was corrected in Khvorostyanov and Curry to

  $$\Delta g^{\#}[\mathrm{J}] = 0.694 \cdot 10^{-12} \cdot [1 + 0.027 \cdot (T_\mathrm{c} + 30) \cdot \exp(0.01 \cdot (T_\mathrm{c} + 30))] . \quad (25)$$

  However, above 243.15 K the Pruppacher and Klett [15] formulation is used.

- Zobrist *et al.* [29]:

  In Zobrist *et al.* an empirical temperature dependent formulation of $\Delta g^{\#}$ is estimated based on measurements of the self-diffusivity by Smith and Kay [85] in the following form:

  $$\Delta g^{\#}[\mathrm{J}] = \frac{k_\mathrm{B} T^2 E}{(T - T^*)^2} \tag{26}$$

  with parameters $E = 892$ K and $T^* = 118$ K. This parameterization is valid in the temperature range of 150 K to 273 K.
  The dataset of the self-diffusivity consists of data between 150 and 157 K and between 250 K and 500 K. The complete dataset can not be fitted by an Arrhenius temperature dependence, because of a much stronger temperature dependence in the cold range. Other methods to fit the temperature dependence are the often used VFT equation and a power-law ansatz. While the VFT equation is able to fit both temperature ranges, the power law fails to fit the cold range like the Arrhenius fit. However, the power law better represents the data above 250 K, thus the ideal method depends on the temperature regime of interest. Zobrist *et al.* [29] used the VFT equation to describe $\Delta g^{\#}$.

- Chen *et al.* [30]:

  In Chen *et al.*, $\Delta g^{\#}$ is used as a fit parameter in CNT. The parameter was estimated for immersion freezing assuming that it is temperature independent over the temperature range of this freezing process (approximately 273.15 to 238.15 K). Because the diffusion of a molecule across phases should not be influenced by the presence of insoluble substances in the water droplet $\Delta g^{\#}$ should be the same for heterogeneous and homogeneous freezing. Moreover it should also be independent of the aerosol type (in case of heterogeneous freezing). However, because it was used as a fit parameter, it varies from dataset to dataset and thus for different aerosol types in this study. The value of $\Delta g^{\#}$ varies from $12.7 \cdot 10^{-20}$ J (soot) to $16 \cdot 10^{-20}$ J (China rose pollen). A value in-between of $14.5 \cdot 10^{-20}$ J is used here as shown in Fig. 1. Besides the result from the fitting method used depends on the estimate of other free parameters, most important on σ_{iw}.

B Methods for estimating n_s

The number of water molecules in contact with the unit area of the ice germ n_s is a surface dependent factor, which is estimated by different authors:

- Fletcher [11]:

  The number of molecules in contact with the unit area of an ice germ or a catalyst surface (as in the case of immersion freezing) can be estimated from the molecular density of water N_l:

  $$n_\mathrm{s}[\mathrm{m}^{-2}] = 3 \cdot 10^{-10} \cdot N_\mathrm{l} \,. \tag{27}$$

  The factor $3 \cdot 10^{-10}$ represents the side dimension of a cube containing one mole of water (approx. $3 \cdot 10^{-29}$ m^3 mol^{-1}). At 273.15 K n_s is approximately 10^{19} m^{-2}.

  The same approximation is used by Young [13] and Khvorostyanov and Curry [86]. Zobrist *et al.* [29] and Chen *et al.* [30] assume that n_s is independent on temperature and use the value at 273.15 K (10^{19} m^{-2}) for the whole temperature range.

- Dufour and Defay [12]:

  In Dufour and Defay n_s is calculated for a spherical germ by:

  $$n_\mathrm{s}[\mathrm{m}^{-2}] = \alpha \cdot r_\mathrm{germ}^{2/3} \,, \tag{28}$$

  where α is a constant. To estimate n_s Dufour and Defay calculated the distance of two neighboring water molecules in tetrahedrally arrangement and came up with 2.69 Å at 277.15 K. For that distance they approximated a value for n_s of $5.21 \cdot 10^{18}$ m^{-2} in the planes (100)(010)(001). In the planes (110)(101)(011) it is $7.4 \cdot 10^{18}$ m^{-2}. For their calculations they used a value of $5.3 \cdot 10^{18}$ m^{-2}. They show, that the higher value of $7.4 \cdot 10^{18}$ m^{-2} changes the nucleation rate by a factor of 1.4. It has a minor effect on the freezing temperature (0.1 K to 0.3 K for small droplets).

  In Pruppacher and Klett [15] as well as Jeffery and Austin [3] (referring to Pruppacher and Klett [15]) a value within the above mentioned range of $5.85 \cdot 10^{18}$ m^{-2} is used.

C Methods for estimating σ_{iw} at the melting point ($\sigma_{iw,0}$)

Due to the fact that $\sigma_{iw,0}$ can only be measured indirectly several measured data exist, which are explained below:

- Kubelka and Prokscha [36]:

  Kubelka and Prokscha used several capillary methods to estimate σ_{iw} from the melting point reduction in the pores of a silica gel using the Thomson equation at approximately 268.15 K. They found an averaged value of $25.4 \cdot 10^{-3}$ J m^{-2}, a minimum value of $21.9 \cdot 10^{-3}$ J m^{-2} and a maximum value of $27.9 \cdot 10^{-3}$ J m^{-2}.

- Skapski *et al.* [37]:

  In 1957 Skapski et al. used a Pyrex tube as a capillary cone in which they measured the ice-water equilibrated interface curvature with a microscope. From the deviation of the melting temperature from 273.15 K they estimated the interfacial tension using the Gibbs-Thomson relation resulting in a rather high value for $\sigma_{iw,0}$ of $44 \cdot 10^{-3} \pm 10 \cdot 10^{-3}$ J m^{-2}. This might be due to inaccurate measurements of the curvature or impurities inside the cone, which might lower the melting point [39].

- Fernandez and Barduhn [87]:

  Fernandez and Barduhn measured the crystal growth of ice crystals in supercooled water with different flow velocities. They found an interfacial tension of $31.8 \cdot 10^{-3} \pm 1.8 \cdot 10^{-3}$ J m^{-2}.

- Coriell *et al.* [88]:

  Coriell *et al.* observed the growth of ice crystal cylinders into supercooled water. The measured growth rates and wavelength of sinusoidal perturbations were then used to estimate $\sigma_{iw,0}$ of $25 \cdot 10^{-3}$ J m^{-2}.

- Ketcham and Hobbs [89]:

  In Ketcham and Hobbs the equilibrium conditions of grain boundary grooves at the liquid-solid interface were investigated and the shape of the grain boundary grooves (grain boundary groove angle) measured. The Young relation [90] was then used to estimate $\sigma_{iw,0}$ from the contact angle leading to $33 \cdot 10^{-3} \pm 3 \cdot 10s^{-3}$ J m^{-2}.

- Jones and Chadwick [38]:

  Jones and Chadwick also used grain boundary measurements, but found a quite different value of $\sigma_{iw,0}$ of $41 \cdot 10^{-3} \pm 9 \cdot 10^{-3}$ J m^{-2}. The measurement was therefore redone in Jones [91] leading to a value of $44 \cdot 10^{-3} \pm 10 \cdot 10^{-3}$ J m^{-2}. Since the error of this measurement is large, the lower value by Ketcham and Hobbs is almost entirely inside the uncertainty range of Jones [91]. The used technique might not work for materials with different thermal conductivities in the liquid and solid phase as in the case of water [39].

- Hardy [39]:

  Similar as in Ketcham and Hobbs [89] and Jones and Chadwick [38] the equilibrium shape of grain boundary grooves at a stabilized melt-crystal interface is observed with a slightly different experimental setup compared to Ketcham and Hobbs [89]. Different from Ketcham and Hobbs [89] $\sigma_{iw,0}$ is indirectly estimated using the analysis from Nash and Glicksman [92]. It results in a value of $29.1 \cdot 10^{-3} \pm 0.8 \cdot 10^{-3}$ J m^{-2}. The measurement of $\sigma_{iw,0}$ by Hardy [39] is considered as the most reliable (*e.g.* Gránásy *et al.* [40]).

- Hillig [93]:

  Hillig used fine-pore cellulose acetate filters, with pore sizes corresponding to the minimum gas pressure allowing bubbling through the water-wetted filters. The corresponding supercooling was measured. From the proportionality between the supercooling and the gas pressure the interfacial tension was calculated. The measurement was repeated for different filter types leading to an average value of $\sigma_{iw,0}$ of $31.7 \cdot 10^{-3} \pm 2.7 \cdot 10^{-3}$ J m^{-2}.

Additionally to measured values some studies did theoretical calculation to estimate σ_{iw}. Thus Volmer [94] suggested to estimate $\sigma_{iw,0}$ based on the assumption that the relation of σ_{iw} to the latent heat of melting L_m is equivalent to the relation of σ_{wa} to the latent heat of vaporization L_v. The approach was used by Krastanow [95]. However, assuming L_v to be constant did result in a wrong temperature behavior of σ_{iw}. The calculated values of Krastanow [95] were later corrected by McDonald [35] using a temperature dependent L_v parameterization. Only the corrected values are plotted in Fig. 2.
Turnbull [96] used a similar approach and did relate σ_{iw} to the heat of melting per unit area and thus estimated $\sigma_{iw,0}$ for different materials including water.

Moreover Oura [97] estimated σ_{iw} from nucleation measurements of Schaefer [69] and Smith-Johannsen [98] by using the formulation of Turnbull and Fisher [10]. He found a value of $18.5 \cdot 10^{-3}$ J m^{-2} at 253.15 K by theoretical considerations.

Another approach was suggested by Born and Stern [99]. It is based on the lattice energy of the ice crystal (cleavage work), which is computed from the energy of hydrogen bonds and Antonoffs rule [100]. Using this method Mason [101] estimated a value for σ_{iw} of $22 \cdot 10^{-3}$ J m^{-2} at 233.15 K. Briegleb [102] re-estimated the energy of the hydrogen bonds at the surface and thus the interfacial tension σ_{iw}. McDonald [35] reviewed the method of Mason and suggested that the energy of hydrogen

bonds at the surface calculated from the sublimation heat has to be corrected and the distortion energy has to be taken into account leading to new estimates for the temperature range from 273.15 to 223.15 K. However, the general assumption, specifically the Antonoffs rule [100], for the calculation is criticized by Ouchi [103].

Gilra and Dass [104] followed another theoretical approach by using precrystallization theory. They calculated low values of $13 \cdot 10^{-3}$ J m^{-2} and $10 \cdot 10^{-3}$ J m^{-2} at 263.15 K and 253.15 K respectively.

Manka *et al.* [49] found an interfacial tension of $15.6 \cdot 10^{-3}$ J m^{-2} in the temperature range from 202 to 215 K from nucleation rate measurements using the analysis from Murray *et al.* [43].

D Methods for estimating $\sigma_{\mathrm{iw}}(T)$

The different forms of $\sigma_{\mathrm{iw}}(T)$ found in literature stem from the use of either a macroscopic value from the list above in combination with a theoretical temperature dependence, a theoretical approach only, a macroscopic value in combination with nucleation measurements, the use of nucleation measurements only or the use of molecular simulations. The estimates for the interfacial tension are therefore dependent on the chosen macroscopic value, the nucleation rate dataset used for fitting, the theoretical assumption of the temperature dependence or the type of molecular model. Some descriptions of all methods will be compared in the following.

- Young relation (1805):

  Youngs semi-empirical relation is based on the mechanical equilibrium conditions of a drop on a solid surface. In this case the interfacial tension between the solid and air (σ_{sa}) is in balance with the interfacial tension between solid and water (σ_{sw}) and the one between water and air (σ_{wa}) multiplied by the cosine of the contact angle θ between the drop and the substrate:

  $$\sigma_{\mathrm{wa}} \cdot \cos\theta = \sigma_{\mathrm{sa}} - \sigma_{\mathrm{sw}} \ . \tag{29}$$

  For θ going towards zero Eq. (29) can be used, following Antonoff, to indirectly calculate σ_{iw} from σ_{ia} and σ_{wa} as they are in equilibrium:

  $$\sigma_{\mathrm{iw}} = \sigma_{\mathrm{ia}} - \sigma_{\mathrm{wa}} \ . \tag{30}$$

  σ_{wa} can be found in Pruppacher and Klett [15]. The formulation of Pruppacher and Klett [15] is taking into account the singularity behavior of water near 228.15 K. σ_{ia} is given *e.g.* in Hale and Plummer [105].

- Ouchi [103]:

  Ouchi derived the temperature dependence of σ_{iw} based on thermodynamics. He assumed that the interface of liquid and ice is a layer of the same amount of ice and water molecules. In this layer the mean internal energy per molecule is

  $$U = \frac{1}{2} \cdot (2U_{\mathrm{w}} + 2U_{\mathrm{i}}) = \Delta U + 2U_{\mathrm{i}}$$

  with ΔU being the difference of the internal energy per molecule related to the different phases $U_{\mathrm{w}} - U_{\mathrm{i}}$.

  Due to mixing of molecules with different phases the entropy is changing. For a large number of molecules (n) the entropy (S) becomes

  $$S = n \cdot k_{\mathrm{B}} \cdot \log(2) \ .$$

As the free energy (F) is defined as $F = U - TS$, the interfacial free energy per molecule is equal to $F_{\text{molecule}} = U - k_B \cdot \log(2)$. The interfacial free energy (interfacial tension) per unit area of the interface is thus the following:

$$\sigma_{iw}[\text{J m}^{-2}] = \frac{U - k_B \cdot \log(2)}{\left(\frac{V_{ice}}{N_A}\right)^{2/3}} \quad (31)$$

with V_{ice} is the volume of one gram molecule of ice.

- Jacobi [33] and Dufour and Defay [12]:

  Jacobi estimated σ_{iw} from his own dataset by using the theory of Volmer [94] for the phase differences, where σ_{iw} is estimated based on the proportion relation of σ_{iw} to the latent heat of melting L_m compared to σ_{wa} to the latent heat of vaporization L_v. Comparison with nucleation measurements lead to a temperature gradient of:

  $$d\sigma_{iw}/dT = 0.2 \cdot 10^{-3} \text{J m}^{-2} \text{ K}^{-1} \quad (32)$$

  and σ_{iw} =16.1 $\cdot 10^{-3}$ J m^{-2} at 238.15 K.

  In Dufour and Defay [12] σ_{iw} was re-estimated from the same dataset using the method of least squares to a regression line for $d\sigma_{iw}/dT$ resulting in:

  $$d\sigma_{iw}/dT = 0.102 \cdot 10^{-3} \text{J m}^{-2} \text{ K}^{-1} \quad (33)$$

  The value of σ_{iw} was estimated to be 20.24 $\cdot 10^{-3}$ J m^{-2} at 238.15 K.
  This estimate is quite different to the one of Jacobi [33]. The deviation comes mainly from a different formula for the germ radius and a different shape factor (assuming the germ to be a hexagonal prism).

- Wood and Walton [106]:

  In this study Wood and Walton measured the kinetics of homogeneous ice nucleation. By fitting CNT to these measurements they derived σ_{iw} at 236.6 K and $d\sigma_{iw}/dT = 0.211 \cdot 10^{-3} \pm 0.012 \cdot 10^{-3}$ J m^{-2} K^{-1} (in their study denoted as the nucleation parameter ω) resulting in:

  $$\sigma_{iw}[\text{J m}^{-2}] = \sigma_{iw,0} + d\sigma_{iw}/dT \cdot T_c \quad (34)$$

  with $\sigma_{iw,0}$ =31.93 $\cdot 10^{-3} \pm 0.44 \cdot 10^{-3}$ J m^{-2}.

- Eadie [7]:

  Eadie gave a full theoretical description of homogeneous nucleation based on a statistical model for liquid water. The basis of the model is the theoretical framework from Némethy and Scheraga [107], where the specific interfacial tension is a variable of the molecular interactions at the ice-water interface. σ_{iw} is obtained as a function of supercooling (see Table 6). For a hexagonal plate a value of 23.42 $\cdot 10^{-3}$ J m^{-2} was determined at a temperature of 238.15 K. The estimate of σ_{iw} is limited by the idealized model used.

Table 6 Specific σ_{iw} computed by Eadie [7]

T_c	Basal face σ_{iw} [10^{-3} J m^{-2}]	Prism face σ_{iw} [10^{-3} J m^{-2}]
0	24.4	26.02
-10	23.76	25.33
-20	23.20	24.74
-30	22.69	24.19
-40	22.19	23.66
-50	21.67	23.11

- DeMott and Rogers [108]:

  Nucleation rate measurements were used to estimate σ_{iw} from CNT. In the temperature range between 239.15 K and 233.15 K a constant value of 22.5 $\cdot 10^{-3}$ J m^{-2} was found to best reproduce the data. Extending the range to 243.15 K and taking the temperature dependence into account yields:

  $$\begin{aligned}\sigma_{iw}[\text{J m}^{-2}] &= 28 \cdot 10^{-3} \text{J m}^{-2} \\ &\quad + 0.167 \cdot 10^{-3} \text{J m}^{-2} \,^{\circ}\text{C}^{-1} \cdot T_c \quad (35)\end{aligned}$$

- Pruppacher and Klett [15]:

  Pruppacher and Klett used an estimate of $\sigma_{iw,0}$ based on unpublished data on latent heat of melting in combination with an educated guess about the temperature dependence. It is expressed by a polynomial expression [Eq. (5-47a) and Eq. (5-47b) in the textbook]:

  Between 237.15 and 273.15 K:

  $$\begin{aligned}\sigma_{iw}[\text{J m}^{-2}] &= 28 \cdot 10^{-3} \text{J m}^{-2} \\ &\quad + 0.25 \cdot 10^{-3} \text{J m}^{-2} \,^{\circ}\text{C}^{-1} \cdot T_c \quad (36)\end{aligned}$$

  And between 237.15 and 229.15 K:

  $$\begin{aligned}\sigma_{iw}[\text{J m}^{-2}] &= (189.081 \text{ J m}^{-2} \\ &\quad + 13.1625 \text{ J m}^{-2} \,^{\circ}\text{C}^{-1} \cdot T_c \\ &\quad + 0.3469 \text{ J m}^{-2} \,^{\circ}\text{C}^{-2} \cdot T_c^2 \\ &\quad + 3.125 \cdot 10^{-3} \text{ J m}^{-2} \,^{\circ}\text{C}^{-4} \cdot T_c^4) \\ &\quad \cdot 10^{-3} \,. \quad (37)\end{aligned}$$

  This formulations are also used by *e.g.* Chen *et al.* [30] and Khvorostyanov and Sassen [19].

- Jeffery and Austin [3]:

  The interfacial tension σ_{iw} in Jeffery and Austin [3] is calculated empirically by a relation which is based on Turnbull [96]. It is expressed as follows:

  $$\sigma_{iw}[\mathrm{J\ m^{-2}}] = k_T \cdot L_m \cdot \rho_i^{2/3} \cdot N_A^{-1/3} - k_\sigma \cdot T\ , \qquad (38)$$

  where k_T is a constant with a value of 0.32 for water, L_m the latent heat of melting, ρ_i the surface density of ice, N_A the Avogadro constant and $k_\sigma = 0.00009$ J m^{-2} K^{-1} another constant estimated by Jeffery and Austin through fitting CNT based nucleation rates to observations. The latent heat of melting is expressed through the change of the specific entropy (s) by the equation of state $L_m = T(s_w - s_i)$, where the specific entropy of water (s_w) is the inverse change of the specific free energy (f) with temperature $s_w = -\left(\frac{\partial f}{\partial T}\right)_{1/\rho_w}$ and the specific entropy of ice (s_i) is $s_i = 1.885 \cdot \log(T) + 0.132 \cdot T - 5.115$, which results from the integration of the heat capacity of ice [3,15].

- Taborek [109] and Gránásy *et al.* [40]:

  In Taborek homogeneous nucleation rate measurements were used to estimate σ_{iw} from CNT. The best fit at 236 K resulted in a interfacial tension of $28.3 \cdot 10^{-3}$ J m^{-2} with a temperature dependence of $d\sigma_{iw}/dT = 0.1 \cdot 10^{-3}$ J m^{-2} K^{-1} leading to a value of $31.9 \cdot 10^{-3}$ J m^{-2} at 273.15 K. $\Delta g^{\#}$ was held constant at $3.4 \cdot 10^6$ J, which resulted from low-viscosity measurements from Hallett [76]. As the nucleation rate in the investigated temperature range is dominated by the interfacial tension, this simplification causes only minor uncertainties. However, note that the value is very small compared to other literature estimates (see Appendix A).

  Gránásy *et al.* [40] used a continuum model instead of the CNT to estimate σ_{iw} from nucleation measurements. The approach stems from a generalization of density functional theories and is the single-order-parameter Cahn-Hilliard approach. They reanalyzed the data from Taborek [109]. The interfacial tension at $T =$ 236 K was estimated to be approx. $24.8 \cdot 10^{-3}$ J m^{-2}, which is slightly lower then the estimate by Taborek [109]. However they found the same temperature dependence, so that the extrapolated value at $T = 273$ K is $27.1 \cdot 10^{-3} \pm 0.2 \cdot 10^{-3}$ J m^{-2}. Gránásy *et al.* mention that the crystal in their modelanalysis could be described with bulk properties in the temperature range of the measurement data.

- Zobrist *et al.* [29]:

  σ_{iw} is used as a fit parameter in Zobrist *et al.* [29]. CNT is fitted to experimental nucleation rates from Pruppacher and Klett [15], Krämer *et al.* [110], Duft and Leisner [66], Benz *et al.* [111], Stöckel *et al.* [112] and Kabath *et al.* [113]. For the formulation of the nucleation rate, Eq. (13), is used with a kinetic prefactor $Z = 1$ and $N_l = 3.1 \cdot 10^{28}$ m^{-3} for the volume number density of water molecules in the liquid. The resulting formula for σ_{iw} is the following:

  $$\begin{aligned}\sigma_{iw}[\mathrm{J\ m^{-2}}] &= 10^{-2}\mathrm{J\ m^{-2}} \cdot [3.298 \\ &\quad + 1.2048 \cdot \frac{T - T_0}{T_0} \\ &\quad - 46.705 \cdot \left(\frac{T - T_0}{T_0}\right)^2]\ . \qquad (39)\end{aligned}$$

  It is valid in the temperature range between 229 and 238 K. However, the extrapolation to 273.15 K yields $32.98 \cdot 10^{-3}$ J m^{-2} and fits to the measured value of Hobbs et al., indicating that the formula can be used over this whole temperature range.

- Huang and Bartell [6] and Murray *et al.* [43]:

  Huang and Bartell proposed that due to lower free energy barrier metastable cubic ice forms first after the phase transition. At homogeneous freezing temperatures it rapidly transforms into the stable hexagonal structure. This assumption is also made by Murray *et al.* [43]. Both estimate σ_{iw} based on their nucleation measurements by fitting the following formula:

  $$\sigma_{iw} = \sigma_{iw}(T_{ref}) \cdot \left(\frac{T}{T_{ref}}\right)^n\ . \qquad (40)$$

  Huang and Bartell [6] got a result of $n = 0.3$ and $\sigma_{iw}(T_{ref}) = 21.55 \cdot 10^{-3}$ or $21.72 \cdot 10^{-3}$ J m^{-2} at $T_{ref} = 200$ K depending on the used dataset (in Fig. 2 the average is used). Murray *et al.* [43] report $n = 0.97$ and $\sigma_{iw}(T_{ref}) = 20.8 \cdot 10^{-3} \pm 1.2 \cdot 10^{-3}$ J m^{-2} at T_{ref} = 235.8 K by plotting the logarithm of the measured nucleation rate against $\mathrm{T}^{-3}(\ln S_i)^2$ [see Eq. (8) in Murray *et al.*, 2010]. As the structure of ice is assumed to be cubic here, a direct comparison to other values of σ_{iw} for hexagonal ice is difficult. Assuming the structure of the ice to be hexagonal yields $\sigma_{iw}(T_{ref}) = 26.8 \cdot 10^{-3} \pm 0.5 \cdot 10^{-3}$ J m^{-2}.

- Chukin *et al.* [77]:

  Chukin *et al.* used a parameterization for σ_{iw} based on Pruppacher and Klett [15] and Berkyaev [114]:

  $$\begin{aligned}\sigma_{iw}[\mathrm{J\ m^{-2}}] &= -0.0397875\ \mathrm{J\ m^{-2}} \\ &\quad + 0.00025\ \mathrm{J\ m^{-2}\ K^{-1}} \cdot T\ . \qquad (41)\end{aligned}$$

  It is valid from 233 K to 273 K.

- Němec [115]:

  σ_{iw} was estimated by fitting nucleation measurement data to CNT in the temperature range of 200-240 K, leading to:

$$\sigma_{iw}[\mathrm{J\ m^{-2}}] = \sigma_{iw,0} \cdot \left(\frac{T}{235.8}\right)^{n} \tag{42}$$

  with $\sigma_{iw,0} = 23.24 \cdot 10^{-3} \pm 1.1 \cdot 10^{-3}$ J m^{-2} and the exponent $n = 0.35$. The nucleation measurements, which were used, were the high pressure measurements from Huang and Bartell [6] and Manka *et al.* [49], the dataset from Hagen *et al.* [5] and the dataset from Stan *et al.* [116]. The pressure dependence of the nucleation rate was explicitly described and taken into account.

  The use of molecular models to simulate the molecular dynamics and thermodynamics has only recently become feasible. These models are explicitly simulating molecular mechanics of water molecules building clusters. They are classified with respect to the amount of points describing one water molecule *i.e.* the interaction between water molecules. Depending on the number of points used, the structure and other features, *e.g.* the polarization of the water molecules, can be represented in the model. One of the simplest models is the TIP4P model of water. It is used in nearly all of the following studies from which the results for σ_{iw} are summarized. The abbreviation stands for "4-point-transferable-intermolecular-potential". The four points refer to both hydrogen atoms, the oxygen atom and the negative charge from the oxygen atom, which is treated separately from the atom and placed near the oxygen at the dipole axis. The angle, shape and body of the water molecule is rigid without any intermolecular forces. Some subversions of the TIP4P model exist, which are the TIP4P-Ew model, using Ewald summation, the TIP4P/Ice model, which is specifically designed for ice, and the TIP4P/2005 model, which is capable to simulate the whole phase diagram of condensed water.
  Results from these models for the estimation of σ_{iw} are given in the following. It should be mentioned that the values of σ_{iw} can be quite different in the case of a planar calculation of σ_{iw} compared to a molecular σ_{iw}.

- Digilov [41]:

  Digilov used Monte Carlo simulations to model the liquid-solid interface and the atomic disordering in the solid-liquid transition zone. From that, the potential function of the interplanar adhesion can be estimated and used to find a relation for σ_{iw} based on the empirical Turnbull rule, where σ_{iw} is correlated with the melting point temperature (T_0) and the latent heat of melting at T_0. The relation found scales with T_0 and the atomic volume ($\Omega_{sm}^{\frac{2}{3}}$):

$$\sigma_{iw,0} \approx \frac{3}{2} \cdot \frac{k_B T_0}{\Omega_{sm}^{\frac{2}{3}}} \cdot \delta^2 \cdot \exp\left(\frac{L_m(T_0)}{3k_B T_0}\right) \tag{43}$$

$$\approx \frac{1}{8} \cdot \frac{3k_B}{S_m} \cdot \exp\left(\frac{S_m}{3k_B}\right) \cdot \frac{L_m(T_0)}{\Omega_{sm}^{\frac{2}{3}}}\,, \tag{44}$$

  where δ is a displacement factor with a value between 0.5 (lower limit for σ_{iw}) and 0.7. The second form of the equation is equivalent to the Turnbull rule. It yields a value of $38.7 \cdot 10^{-3}$ J m^{-2} at T_0 (Ice hcp).

- Davidchack *et al.* [117]:

  In Davidchack *et al.* an extended cleaving method was used, meaning that separate liquid and solid water systems were cleaved and both cleaving potentials were merged to one interface to study the planar interfacial tension. The authors concluded from the simulations that σ_{iw} could be due to the short-range packing interaction between water molecules. They did the simulation with the TIP4P, the TIP4P-Ew and the TIP5P-E model setup leading to similar values of $\sigma_{iw,0}$ of $26.5 \cdot 10^{-3}$, $27.6 \cdot 10^{-3}$ and $28.9 \cdot 10^{-3}$ J m^{-2}, respectively.

- Reinhardt and Doye [72]:

  Reinhardt and Doye used a hybrid Monte Carlo molecular simulation of TIP4P/2005 to estimate σ_{iw}. At a temperature of 240 K, σ_{iw} was found to be approximately $24 \cdot 10^{-3}$ J m^{-2} for monatomic water and $24.5 \cdot 10^{-3}$ J m^{-2} for a basal plane of TIP4P ice. The temperature dependence of σ_{iw} is described by the change in entropy, which occurs per unit area when forming an interface:

$$\left(\frac{\partial \sigma_{iw}}{\partial T}\right)_p = -S\,. \tag{45}$$

  The change of internal entropy S was found to be $0.18 \cdot 10^{-3}$ J m^{-2}K^{-1}.

- Sanz *et al.* [50]:

  Sanz *et al.* used the TIP4P model to simulate an ice Ih cluster surrounded by supercooled water in the temperature range from 258.15 K to 238.15 K. The information gained about the critical cluster was then combined with CNT to estimate σ_{iw} as the size of the critical cluster is strongly correlated with the interfacial tension. The clusters had a size of 600 to 8000 molecules (radius 1.7 to 4 nm), from which the plane in contact with the supercooled liquid and thus σ_{iw} was calculated. Sanz

et al. derived a value of $28.7 \cdot 10^{-3}$ J m^{-2} at the melting point and a temperature dependence of $d\sigma_{iw}/dT = 0.18 \cdot 10^{-3}$ J m^{-2} K^{-1}.

To counteract the problem that σ_{iw} is a macroscopic property and might be different in case of small clusters of water molecules, Bogdan [118] estimated the curvature effect on σ_{iw} following Tolman [119]. As a basis he used the formulation of Dufour and Defay [12] and the Gibbs [17] relations. He found that σ_{iw} decreases with curvature (resulting in smaller critical clusters), which on the other hand then increases the probability of nucleation.

Remarks and typographical errors found in the literature. The review of the kinetic and thermodynamic parameters is necessary incomplete due to the large amount of literature on this subject.
One typographical error was found in Pruppacher and Klett [15]: On page 206 n_s (here N_c) has to be $5.85{\cdot}10^{14}$ cm^{-2} and $5.3{\cdot}10^{14}$ cm^{-2} instead of $5.85{\cdot}10^{12}$ cm^{-2} and $5.3{\cdot}10^{12}$ cm^{-2}.
In Taborek [109] $\sigma_{iw,0}$ is different from the value given in Table 3. The value was calculated using the linear slope $d\sigma_{iw}/dT$ and the measured value of σ_{iw} at 236 K and deviates most probably from the original value because $d\sigma_{iw}/dT$ is rounded in the paper to 0.1 J m^{-2} K^{-1}.
Extrapolating the data of Gránásy *et al.* [40] is giving a value of $28.6{\cdot}10^{-3}$ J m^{-2} for $\sigma_{iw,0}$ instead of the extrapolated value in the paper ($27.1{\cdot}10^{-3}$ J m^{-2} $\pm$ $0.2{\cdot}10^{-3}$ J m^{-2}).

Acknowledgments. The authors would like to thank Joel Corbin for discussions and proof-reading, Matteo Tanadini (Tana) and Sarah Grimm for statistical consulting, Thea Schmitt for discussions about homogeneous freezing datasets, Aleksandra Borodina for the help with the Russian literature and the anonymous reviewers for their input and dicussion.

References

1 M. Volmer and A. Weber, *Z. phys. Chem.*, 1926, **119**, 277 – 301.
2 H. R. Pruppacher, *J. Atmos. Sci.*, 1995, **52**, 1924–1933.
3 C. A. Jeffery and P. H. Austin, *J. Geophys. Res.-Atmos.*, 1997, **102**, 25269–25279.
4 I. R. Türkmen, *PhD thesis*, Freie Universität Berlin, 2007.
5 D. E. Hagen, R. J. Anderson and J. L. Kassner, *J. Atmos. Sci.*, 1981, **38**, 1236–1243.
6 J. Huang and L. S. Bartell, *J. Phys. Chem.*, 1995, **99**, 3924–3931.
7 W. J. Eadie, *PhD thesis*, University of Chicago, 1971.
8 A. C. Zettlemoyer, *Nucleation*, Marcel Dekker, Inc., 1969.
9 G. Vali, *Bull. Amer. Meteor. Soc.*, 1985, **66**, 1426–1427.
10 D. Turnbull and J. C. Fisher, *J. Chem. Phys.*, 1949, **17**, 71–73.
11 N. H. Fletcher, *The Physics of Rainclouds*, Cambridge University Press, 1962.
12 L. Dufour and R. Defay, *Thermodynamics of Clouds*, Academic Press, 1963, vol. 6.
13 K. C. Young, *Microphysical Processes in Clouds*, Oxford University Press, 1993.
14 P. G. Debenedetti, *Metastable liquids : concepts and principles*, Princeton University Press, 1996.
15 H. R. Pruppacher and J. D. Klett, *Microphysics of Clouds and Precipitation*, Dordrecht : Kluwer Academic Publishers, 2nd edn, 2000, vol. 18.
16 M. P. Anisimov, *Russ. Chem. Rev.*, 2003, **72**, 591–628.
17 J. W. Gibbs, *The collected works of J. Willard Gibbs*, Yale University Press, 1948, vol. 1.
18 R. R. Rogers and M. K. Yau, *A short course in cloud physics*, Pergamon Press, 1989.
19 V. Khvorostyanov and K. Sassen, *Geophys. Res. Lett.*, 1998, **25**, 3155–3158.
20 V. I. Khvorostyanov and J. A. Curry, *Geophys. Res. Lett.*, 2000, **27**, 4081–4084.
21 S. Balibar and F. Caupin, *C. R. Phys.*, 2006, **7**, 988–999.
22 Y. B. Zeldovich, *J. Exp. Theor. Phys. (USSR)*, 1942, 525–538.
23 L. A. Bulavin, T. V. Lokotosh and N. P. Malomuzh, *J. Mol. Liq.*, 2008, **137**, 1–24.
24 R. G. Dorsch and B. Boyd, *Tech. Notes nat. adv. Comm. Aero*, 1951, pp. 14.
25 C. J. Fecko, J. D. Eaves, J. J. Loparo, A. Tokmakoff and P. L. Geissler, *Science*, 2003, **301**, 1698–1702.
26 S. Glasstone, K. Laidler and H. Eyring, *The theory of rate processes*, McGraw Hill, New York, 1941.
27 K. Krynicki, C. D. Green and D. W. Sawyer, *Faraday Discuss. Chem. Soc.*, 1978, **66**, 199–208.
28 J. H. Wang, C. V. Robinson and I. S. Edelman, *J. Am. Chem. Soc.*, 1953, **75**, 466–470.
29 B. Zobrist, T. Koop, B. P. Luo, C. Marcolli and T. Peter, *J. Phys. Chem. C*, 2007, **111**, 2149–2155.
30 J.-P. Chen, A. Hazra and Z. Levin, *Atmos. Chem. Phys.*, 2008, **8**, 7431–7449.
31 C. Hoose and O. Möhler, *Atmospheric Chemistry and Physics Discussions*, 2012, **12**, 12531–12621.
32 A. Tabazadeh, Y. S. Djikaev and H. Reiss, *Proceedings of the National Academy of Sciences*, 2002, **99**, 15873–15878.
33 W. Jacobi, *Z. Naturforsch. Pt. A*, 1955, **10**, pp. 322.
34 G. T. Butorin and V. P. Skripov, *Sov. Phys. Crystallogr.*, 1972, **17**, 379–384.
35 J. E. McDonald, *J. Meteor.*, 1953, **10**, 416–433.
36 P. Kubelka and R. Prokscha, *Kolloid Z.*, 1944, **109**, 79–85.
37 A. Skapski, R. Billups and A. Rooney, *J. Chem. Phys.*, 1957, **26**, 1350–1351.
38 D. R. H. Jones and G. A. Chadwick, *Philos. Mag.*, 1970, **22**, 291–300.
39 S. C. Hardy, *Philos. Mag.*, 1977, **35**, 471–484.
40 L. Gránásy, T. Pusztai and P. F. James, *J. Chem. Phys.*, 2002, **117**, 6157–6168.
41 R. M. Digilov, *Surf. Sci.*, 2004, **555**, 68 – 74.
42 D. M. Murphy and T. Koop, *Quart. J. Roy. Meteor. Soc.*, 2005, **131**, 1539–1565.
43 B. J. Murray, S. L. Broadley, T. W. Wilson, S. J. Bull, R. H. Wills, H. K. Christenson and E. J. Murray, *Phys. Chem. Chem. Phys.*, 2010, **12**, 10380–10387.
44 J. A. Goff, *Trans. Am. Soc. Heating Air-Cond. Eng.*, 1957, **63**, 347–354.
45 World Meteorological Organization, in *General meteorological standards and recommended practices, Appendix A*, 2000, vol. 49.
46 K. C. Young, *J. Atmos. Sci.*, 1974, **31**, 768–776.
47 B. Riechers, F. Wittbracht, A. Hutten and T. Koop, *Phys. Chem. Chem. Phys.*, 2013, **15**, 5873–5887.
48 L. S. Bartell and Y. G. Chushak, *Water in Confining Geometries*, Springer Berlin Heidelberg, 2003, pp. 399–424.
49 A. Manka, H. Pathak, S. Tanimura, J. Wolk, R. Strey and B. E. Wyslouzil, *Phys. Chem. Chem. Phys.*, 2012, **14**, 4505–4516.

50 E. Sanz, C. Vega, J. R. Espinosa, R. Caballero-Bernal, J. L. F. Abascal and C. Valeriani, *J. Am. Chem. Soc.*, 2013, **135**, 15008–15017.
51 E. K. Bigg, *Quart. J. Roy. Meteor. Soc.*, 1953, **79**, 510–519.
52 E. K. Bigg, *Proc. Phys. Soc., Sect. B*, 1953, **66**, 688.
53 A. E. Carte, *Proc. Phys. Soc., Sect. B*, 1956, **69**, 1028.
54 S. C. Mossop, *P. Phys. Soc. B*, 1955, **68**, 193.
55 E. J. Langham and B. J. Mason, *Proceedings of the Royal Society of London. Series A. Mathematical and Physical Sciences*, 1958, **247**, 493–504.
56 T. E. Hoffer, *J. Meteor.*, 1961, **18**, 766–778.
57 S. E. Wood, M. B. Baker and B. D. Swanson, *Rev. Sci. Instrum.*, 2002, **73**, 3988–3996.
58 B. H. Larson and B. D. Swanson, *J. Phys. Chem. A*, 2006, **110**, 1907–1916.
59 M. E. Earle, T. Kuhn, A. F. Khalizov and J. J. Sloan, *Atmos. Chem. Phys.*, 2010, **10**, 7945–7961.
60 D. A. Knopf and Y. J. Rigg, *J. Phys. Chem. A*, 2011, **115**, 762–773.
61 C. R. Hoyle, V. Pinti, A. Welti, B. Zobrist, C. Marcolli, B. Luo, A. Höskuldsson, H. B. Mattsson, O. Stetzer, T. Thorsteinsson, G. Larsen and T. Peter, *Atmos. Chem. Phys.*, 2011, **11**, 9911–9926.
62 T. Kuhn, M. E. Earle, A. F. Khalizov and J. J. Sloan, *Atmos. Chem. Phys.*, 2011, **11**, 2853–2861.
63 F. Broto, D. Clausse, L. Babin and M. Clausse, *Colloid Polym. Sci.*, 1979, **257**, 302–308.
64 F. Broto and D. Clausse, *J. Phys. C*, 1976, **9**, 4251.
65 D. A. Knopf, P. A. Alpert, B. Wang and J. Y. Aller, *Nature Geosci*, 2011, **4**, 88–90.
66 D. Duft and T. Leisner, *Atmos. Chem. Phys.*, 2004, **4**, 1997–2000.
67 D. Rzesanke, J. Nadolny, D. Duft, R. Müller, A. Kiselev and T. Leisner, *Phys. Chem. Chem. Phys.*, 2012, **14**, 9359–9363.
68 M. Bayardelle, *Comptes Rendus Hebdomadaires des Seances de l Academie des Sciences*, 1954, **239**, 988–989.
69 V. J. Schaefer, *Ind. Eng. Chem.*, 1952, **44**, 1300–1304.
70 M. J. Lindstrom and D. M. Bates, *Biometrics*, 1990, **46**, 673–687.
71 J. C. Pinheiro and D. M. Bates, *Mixed-effects models in S and S-PLUS*, Springer, 2004.
72 A. Reinhardt and J. P. K. Doye, *J. Chem. Phys.*, 2013, **139**, 1–2.
73 M. L. Huber, R. A. Perkins, A. Laesecke, D. G. Friend, J. V. Sengers, M. J. Assael, I. N. Metaxa, E. Vogel, R. Mares and K. Miyagawa, *J. Phys. Chem. Ref. Data*, 2009, **38**, 101–125.
74 N. E. Dorsey, *Properties of ordinary water-substance in all its phases : Water-vapor, water and all the ices*, New York : Reinhold, 1940, vol. 81.
75 C. H. Collie, J. B. Hasted and D. M. Ritson, *Proc. Phys. Soc.*, 1948, **60**, 145.
76 J. Hallett, *Proc. Phys. Soc.*, 1963, **82**, 1046.
77 V. V. Chukin, E. A. Pavlenko and A. S. Platonova, *Russ. Meteorol. Hydrol.*, 2010, **35**, 524–529.
78 R. Mills, *J. Phys. Chem.*, 1973, **77**, 685–688.
79 R. Mills, *Berich. Bunsen Gesell.*, 1971, **75**, 195–199.
80 K. T. Gillen, D. C. Douglass and M. J. R. Hoch, *J. Chem. Phys.*, 1972, **57**, 5117–5119.
81 H. R. Pruppacher, *J. Chem. Phys.*, 1972, **56**, 101–107.
82 F. X. Prielmeier, E. W. Lang, R. J. Speedy and H.-D. Lüdemann, *Phys. Rev. Lett.*, 1987, **59**, 1128–1131.
83 K. R. Harris and L. A. Woolf, *J. Chem. Soc., Faraday Trans. 1*, 1980, **76**, 377–385.
84 E. J. Jensen, O. B. Toon, D. L. Westphal, S. Kinne and A. J. Heymsfield, *J. Geophys. Res.-Atmos.*, 1994, **99**, 10421–10442.
85 R. S. Smith and B. D. Kay, *Nature*, 1999, **398**, 788–791.
86 V. I. Khvorostyanov and J. A. Curry, *J. Atmos. Sci.*, 2004, **61**, 2676–2691.
87 R. Fernandez and A. J. Barduhn, *Desalination*, 1967, **3**, 330–342.
88 S. R. Coriell, S. C. Hardy and R. F. Sekerka, *J. Cryst. Growth*, 1971, **11**, 53–67.
89 W. M. Ketcham and P. V. Hobbs, *Philos. Mag.*, 1969, **19**, 1161–1173.
90 T. Young, *Philos. Trans. R. Soc.*, 1805, **95**, 65–87.
91 D. R. H. Jones, *J. Mater. Sci.*, 1974, **9**, 1–17.
92 G. E. Nash and M. E. Glicksman, *Philos. Mag.*, 1971, **24**, 577–592.
93 W. B. Hillig, *J. Cryst. Growth*, 1998, **183**, 463–468.
94 M. Volmer, *Kinetik der Phasenbildung*, Steinkopff-Verlag, 1939.
95 L. Krastanow, *Meteor. Z.*, 1941, **58**, 37–45.
96 D. Turnbull, *J. Appl. Phys.*, 1950, **21**, 1022–1028.
97 H. Oura, *J. Phys. Soc. Japan*, 1950, **5**, 277–279.
98 R. Smith-Johannsen, *Science*, 1948, **108**, 652–654.
99 M. Born and O. Stern, *Sitzungsberichte der Königlich Preussischen Akademie der Wissenschaften*, 1919, 901–913.
100 G. Antonoff, *Ann. Physik*, 1939, **35**, 84–96.
101 B. J. Mason, *Quart. J. Roy. Meteor. Soc.*, 1952, **78**, 22–27.
102 G. Briegleb, *Zwischenmolekulare Kräfte*, 1949.
103 K. Ouchi, *Sci. Rep. Tohoku Univ.*, 1954, **6**, 43–61.
104 N. K. Gilra and N. Dass, *J. Phys. Soc. Jpn.*, 1968, **24**, 910–912.
105 B. N. Hale and P. L. M. Plummer, *J. Chem. Phys.*, 1974, **61**, 4012–4019.
106 G. R. Wood and A. G. Walton, *J. Appl. Phys.*, 1970, **41**, 3027–3036.
107 G. Némethy and H. A. Scheraga, *J. Chem. Phys.*, 1962, **36**, 3382–400.
108 P. J. DeMott and D. C. Rogers, *J. Atmos. Sci.*, 1990, **47**, 1056–1064.
109 P. Taborek, *Phys. Rev. B*, 1985, **32**, 5902–5906.
110 B. Krämer, O. Hübner, H. Vortisch, L. Wöste, T. Leisner, M. Schwell, E. Rühl and H. Baumgärtel, *J. Chem. Phys.*, 1999, **111**, 6521–6527.
111 S. Benz, K. Megahed, O. Möhler, H. Saathoff, R. Wagner and U. Schurath, *J. Photochem. Photobiol. A*, 2005, **176**, 208–217.
112 P. Stöckel, I. M. Weidinger, H. Baumgärtel and T. Leisner, *J. Phys. Chem. A*, 2005, **109**, 2540–2546.
113 P. Kabath, P. Stöckel, A. Lindinger and H. Baumgärtel, *J. Mol. Liq.*, 2006, **125**, 204–211.
114 V. I. Berkyaev, *L. Gidrometeoizdat*, 1991.
115 T. Němec, *Chem. Phys. Lett.*, 2013, **583**, 64–68.
116 C. A. Stan, G. F. Schneider, S. S. Shevkoplyas, M. Hashimoto, M. Ibanescu, B. J. Wiley and G. M. Whitesides, *Lab. Chip*, 2009, **9**, 2293–2305.
117 R. L. Davidchack, R. Handel, J. Anwar and A. V. Brukhno, *J. Chem. Theory Comput.*, 2012, **8**, 2383–2390.
118 A. Bogdan, *J. Chem. Phys.*, 1997, **106**, 1921–1929.
119 R. C. Tolman, *J. Chem. Phys.*, 1948, **16**, 758–774.

Table 7 List of symbols

Symbol	SI Unit	Description
A	J m^{-2} K^{-1}	Fit parameter for $d\sigma_{\mathrm{iw}}/dT$
B	J	Fit parameter for $\Delta g^{\#}$
C_{prefac}	m^{-3} s^{-1}	Preexponential factor of the nucleation rate
D	m^2 s^{-1}	Self-diffusivity of water
e_{sw}, e_{si}	Pa	Saturation vapor pressure over water and ice, respectively
f, F	J	(Specific) free energy
h	J s	Planck constant
J_{hom}	m^{-3} s^{-1}	Homogeneous nucleation rate
k_{B}	J K^{-1}	Boltzmann constant
K	s^{-1}	Rate of water molecules potentially transferring into an ice germ in the water volume
L_{m}, L_{v}	J kg^{-1}	Latent heat of melting/vaporization
n	-	Number of molecules
n_k, $n_{k,\mathrm{germ}}$	-	Number of water molecules in the ice embryo and germ, respectively
n_{s}	m^{-2}	Number of water molecules in contact with the unit area of the ice germ
N_{A}	mol^{-1}	Avogadro constant
N_{germ}	-	Number of ice germs in the water droplet
N_{l}	m^{-3}	Volume number density of water molecule in liquid water
r_{embryo}, r_{germ}	m	Radius of the ice embryo/ice germ (=critical radius)
R	J mol^{-1} K^{-1}	Universal gas constant
s, S	J	(Specific) entropy
S_{m}	J	Melting entropy
S_{i}	-	Saturation ratio with respect to ice
T	K	Temperature
T_{c}	°C	Temperature in °C (non SI unit)
T_0	K	Melting point of water (273.15 K)
U	J	Internal energy
V_{drop}	m^3	Volume of a water drop
$v_{\mathrm{H_2O}}$	m^3	Volume of a water molecule
v_{ice}	m^3	Volume of a water molecule in the ice embryo
V_{ice}	m^3	Volume of one gram molecule of ice
Z	-	Zeldovich factor
$\Delta g^{\#}$	J	Activation energy barrier
ΔG_k	J	Gibbs free energy barrier
η	m^2 s^{-1}	Viscosity of water
μ_{w}, μ_{i}	J	Chemical potential of water and ice, respectively
ρ_{i}	kg m^{-3}	Surface density of ice
σ_{iw}, σ_{ia}, σ_{wa}, σ_{sa}, σ_{sw}	J m^{-2}	Interfacial tension between ice/water, ice/air, water/air, solid/air, solid/water
$\sigma_{\mathrm{iw},0}$	J m^{-2}	Interfacial tension at the ice water interface at 273.15 K
τ	s	Dielectric relaxation time of water
θ	rad	Contact angle
Φ	s^{-1}	Diffusive molecule flux to the ice germ
$\Omega_{\mathrm{sm}}^{\frac{2}{3}}$	m^2	Surface area per atom at interface